Bioactive Materials 41 (2024) 221–238

Contents lists available at ScienceDirect

Bioactive Materials

journal homepage: www.keaipublishing.com/en/journals/bioactive-materials

Synergistic rheumatoid arthritis therapy by interrupting the detrimental feedback loop to orchestrate hypoxia M1 macrophage polarization using an enzyme-catalyzed nanoplatform

Dong Guo [a,b,1], Hui Liu [a,b,c,1], Sheng Zhao [c], Xinya Lu [a,b], Haoyu Wan [a,b], Yitao Zhao [a,b], Xinzhi Liang [a,b], Anbiao Zhang [a,b], Mengyuan Wu [c], Zhisheng Xiao [a,b], Ning Hu [d], Zhong Li [e], Denghui Xie [a,b,*]

[a] Department of Orthopedic Surgery, Center for Orthopedic Surgery, The Third Affiliated Hospital of Southern Medical University, Guangzhou, 510630, PR China
[b] Guangdong Provincial Key Laboratory of Bone and Joint Degeneration Diseases, Guangzhou, 510630, PR China
[c] Key Laboratory of Luminescence Analysis and Molecular Sensing (Southwest University), Ministry of Education, School of Materials and Energy, Southwest University, Chongqing, 400715, PR China
[d] Department of Orthopaedics, The First Affiliated Hospital of Chongqing Medical University, Chongqing, 400016, PR China
[e] Department of Biomedical Engineering, The Chinese University of Hong Kong, NT, Hong Kong, PR China

ARTICLE INFO

Keywords:
Hypoxia
Oxidative stress
Nanoplatform
Macrophage
Metabolic regulation
Rheumatoid arthritis

ABSTRACT

A detrimental feedback loop between hypoxia and oxidative stress consistently drives macrophage polarization toward a pro-inflammatory M1 phenotype, thus persistently aggravating rheumatoid arthritis (RA) progression. Herein, an enzyme-catalyzed nanoplatform with synergistic hypoxia-relieving and reactive oxygen species (ROS)-scavenging properties was developed using bovine serum albumin-bilirubin-platinum nanoparticles (BSA-BR-Pt NPs). Bilirubin was employed to eliminate ROS, while platinum exhibited a synergistic effect in scavenging ROS and simultaneously generated oxygen. In mice RA model, BSA-BR-Pt NPs treatment exhibited superior effects, resulting in significant improvements in joint inflammation, cartilage damage, and bone erosion, compared to methotrexate, the most widely used antirheumatic drug. Mechanistically, RNA-sequencing data and experimental results elucidated that BSA-BR-Pt NPs induced a re-polarization of hypoxic M1 macrophages to M2 macrophages via switching glycolysis to oxidative phosphorylation through the inhibition of HIF-1α pathway. Collectively, this research for the first time elaborated the underlying mechanism of enzyme-catalyzed nanoplatform in orchestrating macrophage polarization, and identified a novel therapeutic strategy for RA and other inflammatory disorders.

1. Introduction

Rheumatoid arthritis (RA) represents the most common type of chronic inflammatory arthritis that impacts approximately 1 % of the global population, resulting in enduring synovial inflammation, cartilage degeneration and bone erosion. Several novel therapeutic strategies, including gay therapy, have been developed for RA treatment. Gas therapy has shown promise in effectively modulating the RA microenvironment, attenuating inflammation, and promoting bone repair, due to its notable therapeutic efficacy, low systemic adverse effects, and excellent biosafety profile [1–3]. While the precise pathophysiological mechanisms of RA remain incompletely elucidated, inflammation of the synovial lining within the joints is a central feature [4]. Although the advent of targeted antirheumatic drugs has notably improved the clinical outlook in RA patients [5], approximately 40 % of RA patients fail to response to a single agent, and up to 20 % do not respond to any treatment currently available [6]. Thus, a thorough comprehension of RA pathogenesis will be imperative for addressing the variability of the

Peer review under responsibility of KeAi Communications Co., Ltd.
* Corresponding author. Department of Orthopedic Surgery, Center for Orthopedic Surgery, The Third Affiliated Hospital of Southern Medical University, Guangzhou, 510630, PR China.
E-mail address: smuspine@163.com (D. Xie).
[1] DG and HL contributed equally to this work.

https://doi.org/10.1016/j.bioactmat.2024.07.026
Received 25 May 2024; Received in revised form 14 July 2024; Accepted 17 July 2024

disease and overcoming these persistent challenges.

Synovial hypoxia and oxidative stress, triggered by insufficient oxygen supply and excessive reactive oxygen species (ROS) accumulation, were involved in macrophage polarization during the progression of RA [7,8]. Synovial hyperplasia, angiogenesis, and leukocyte extravasation leads to the conversion of the typical synovium into an invasive pannus. The resultant dysregulated microvascular architecture contributes to inadequate oxygen delivery to the synovium, exacerbating the hypoxic environment due to the heightened metabolic activity of the expanding synovial pannus. Hypoxic conditions promoted the accumulation of ROS, identified as crucial pro-inflammatory mediators, thereby exacerbating the progression of RA through enhanced oxidative stress [9]. This phenomenon resulted in the migration of pro-inflammatory M1-polarized macrophages from blood to inflamed synovial tissue, consequently increasing oxygen demand and aggravating hypoxia [10,11]. These findings indicated the detrimental feedback loop between hypoxia and oxidative stress played a critical role in aggravating RA development.

It was well-established that the hypoxia-inducible factor (HIF), known as the primary regulator of oxygen homeostasis, was observed to be upregulated in RA synovial tissue [12]. Increased levels of HIF-1α were found to stimulate the transcription of glycolytic enzymes, leading to an elevation in glycolytic rate and a subsequent reduction in oxidative phosphorylation (OXPHOS) [10]. This shift towards glycolysis favored the development of an M1-polarized macrophage phenotype, as opposed to M2 macrophage polarization [13]. Furthermore, it was evident that

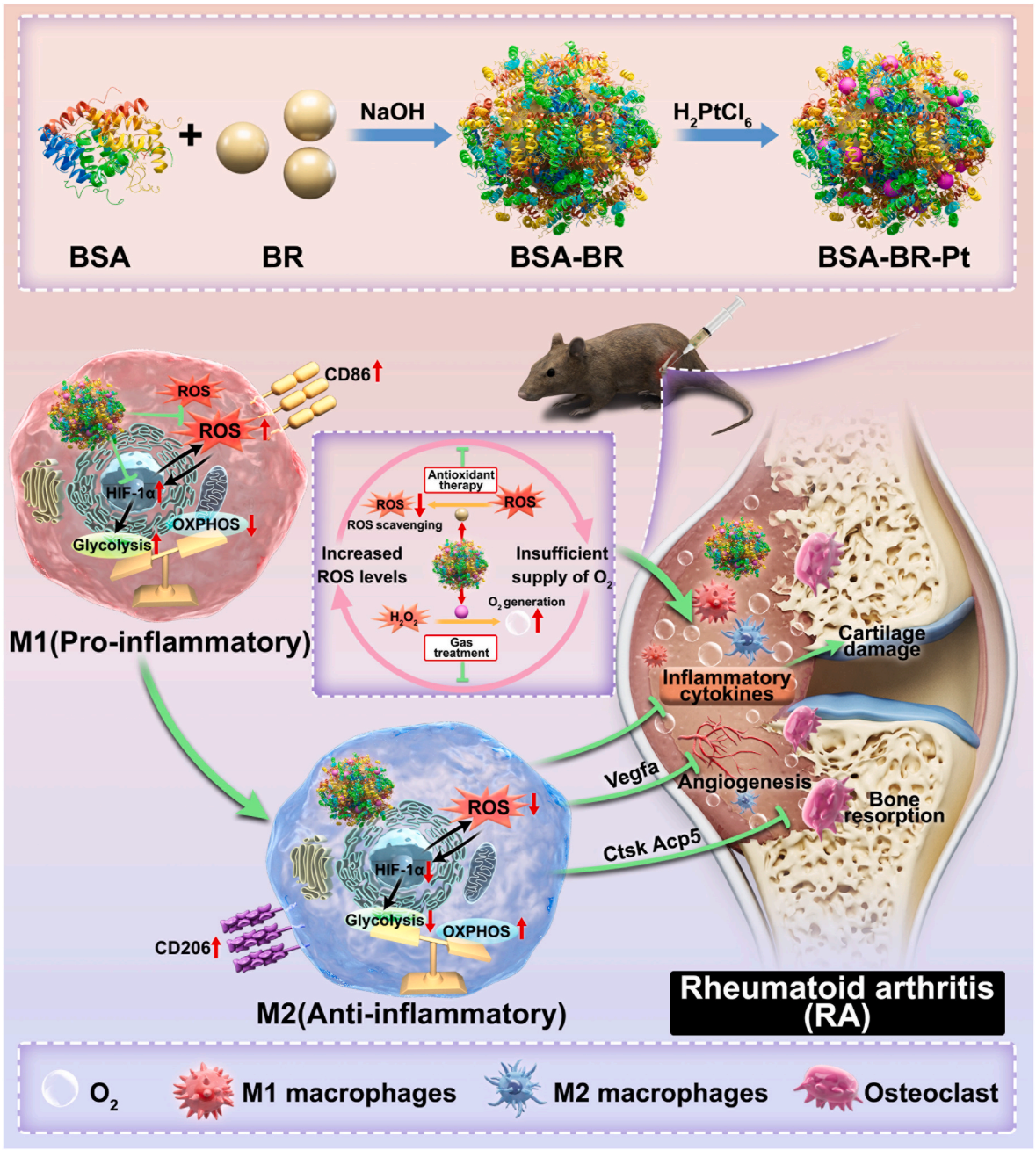

Scheme 1. Schematic depiction of BSA-BR-Pt NPs preparation and therapeutic mechanism against rheumatoid arthritis. The enzyme-catalyzed nanoplatform with synergistic O_2-generating and ROS-scavenging properties reprograms hypoxic M1 macrophages towards M2 via modulating metabolic pathway from glycolysis to oxidative phosphorylation through the HIF-1α pathway. Ultimately, this reprogramming attenuates synovitis, aberrant angiogenesis, cartilage degeneration, and bone erosion, providing a comprehensive treatment approach for RA.

increased ROS level of hypoxic synovium facilitated the polarization of M1 macrophages through decreased OXPHOS in RA patients [14,15]. Taken together, promoting the polarization of hypoxic M1 macrophages towards M2 through the inhibition of glycolysis and the enhancement of OXPHOS may hold promise as a potential target for RA treatment.

Herein, based on reprogramming hypoxic M1 macrophage polarization strategy against RA, we synthesized a kind of enzyme-catalyzed nanoplatform with synergistic hypoxia-relieving and ROS-scavenging properties (Scheme 1). Compared to other reported references, these bilirubin-based nanoparticles were formed through physical interaction rather than chemical bond, featuring green synthesis process and easy drug release [16,17]. Moreover, bilirubin nanoparticles exhibit a favorable safety profile and have been extensively utilized in the treatment of various chronic and acute inflammatory diseases [18]. Platinum had been used as as oxygen-generating nanozyme owing to its cost-effectiveness, excellent stability, and ability for large-scale production [19,20]. The nanoplatform was consequently composed of bovine serum albumin-bilirubin-platinum nanoparticles (BSA-BR-Pt NPs). Bilirubin was incorporated to eliminate ROS, while platinum acted synergistically with bilirubin to scavenge ROS (specifically hydrogen peroxide) and generate O_2 simultaneously. Our findings showed BSA-BR-Pt NPs effectively generated oxygen and synergistically scavenged ROS *in vitro*. Strikingly, superior therapeutic effects were observed in the knee and ankle joint of RA mice with BSA-BR-Pt NPs treatment when compared to methotrexate. Through RNA-sequencing analysis and subsequent findings, we have conclusively demonstrated that BSA-BR-PtS NPs induced a shift from hypoxic M1 macrophages to M2 macrophages by modulating glycolysis towards OXPHOS via the HIF-1a pathway. Our research identified a promising therapeutic strategy for RA utilizing an enzyme-catalytic nanoplatform, and elucidated its underlying mechanism in the treatment of RA. The exploration of this work is expected to provided positive promotion for the clinical relance and translational of such nanomaterials.

2. Materials and methods

2.1. Materials

Bilirubin (BR, 99 %) was brought from Maclin (Shanghai, China). Bovine serum albumin (BSA, ≥98.0 %), chloroplatinic acid solution (8 wt% in H_2O), copper chloride anhydrous ($CuCl_2$, 98 %), reducing glutathione (GSH), and methylene blue (MB) were brought from Aladdin (Shanghai, China). Hydrogen peroxide (H_2O_2, 30 %) was brought from Chuandong Chemical Co., Ltd. (Chongqing, China). Hydrogen peroxide detection kit was brought from Beyotime (Shanghai, China).

2.2. Preparation of BSA-BR-Pt NPs

Firstly, BSA (23.8 mg/mL, 1 mL), H_2O (45.6 mL), and BR (1 mg/mL in 0.01 M NaOH solution, 1 mL) were added to a reaction vessel, and the reaction was ended after stirring for 2.5 h. Then, the BSA-BR nanoparticles (NPs) were purified by dialysis (1 L/time, two times in PBS and one time in DI water) for 24 h, and further by centrifugation at 3000 rpm for 5 min. These obtained BSA-BR NPs were stored at −4 °C for further use.

Then, BSA-BR NPs (1 mg/mL, 10 mL) and H_2PtCl_6 (10 mg/mL, 0.2 mL) were added to a reaction vessel at the mass ratio of 1:0.2. After mixing for 0.5 h, $NaBH_4$ solution (0.5 mg/mL, 0.876 mL) was added into the mixture with the molar ratio of n(H_2PtCl_6) and n($NaBH_4$) at 1:3. The reaction was ended after stirring for 2 h. The mixture was purified by dialysis for 24 h (1 L/time, two times in DI water) and further by centrifugation at 3000 rpm for 5 min. These obtained BSA-BR-Pt NPs were stored at −4 °C for further use.

2.3. Analysis of •OH clearance capacity

Briefly, $CuCl_2$ (2 mg/mL, 1 mL), GSH (20 mM, 1 mL), and PBS (7.4, 1x, 8 mL) were mixed and stirred for 12 h. Then, MB (0.05 mg/mL, 0.5 mL), BSA-BR NPs (final concentrations at 0 ppm, 50 ppm, 100 ppm, 200 ppm, and 400 ppm, respectively), H_2O_2 (20 mM, 1 mL) were added sequentially to the mixture. After that, the mixture (1 mL) was centrifuged at different time points (5 min, 1 h, 2 h, and 4 h), and the supernatant was detected by UV–Vis–NIR spectrophotometer at 664 nm.

2.4. Analysis of H_2O_2 clearance capacity

Different concentrations of BSA-BR NPs and BSA-BR-Pt NPs were added to 200 μM H_2O_2 solution under vortexing. The mixture (1 mL) was centrifuged to collect the supernatant after shaking at 37 °C for 1 h. Subsequently, a hydrogen peroxide detection kit was used to estimate the H_2O_2 levels.

2.5. O_2 generation analysis

Different concentrations of BSA-BR-Pt NPs were added to H_2O_2 solution. The blends were enclosed and agitated in a water bath at a temperature of 37 °C.The fluctuations in dissolved oxygen levels were monitored using an oxygen meter from Ohaus.

2.6. Cell preparation and stimulation

Bone marrowderived macrophages (BMDMs) were isolated from the bone marrow of 6–8-week-old male C57BL/6J, as previously described [21]. Hypoxic conditions were induced by Oxoid AnaeroGen system for 24 h (#AN0025A, Thermo Fisher Scientific, Basingstoke, United Kingdom). Inflammatory stimulation was achieved by treating the BMDMs with 500 ng/mL lipopolysaccharide (LPS) for 24 h (LPS, #HY-D1056, MedChemExpress, Shanghai, China). Following hypoxia and inflammation induction, the BMDMs were treated with BSA, BSA-BR NPs, and BSA-BR-Pt NPs after 12 h.

2.7. Animals and collagen-induced arthritis (CIA) model

Male DBA/1J mice, 7–8 weeks old and weighing 20 ± 2 g, were purchased from GemPharmatech (Nanjing, China), and kept in a clean and sterile environment with free access to food and water. The animal experiments were authorized by the Animal Experimental Committee of the Daoke Pharmaceutical Technology (Guangdong) Co., Ltd (Approval IACUC-DK-2024-04-22-01) and carried out in accordance with the regulations outlined in the National Law on Experimental Animal Utilization (People's Republic of China).

According to a prior study, we established the CIA mice model [22]. Briefly, two mixtures were formed by blending 2 mg/mL bovine type II collagen with an equivalent amount of Complete Freund's Adjuvant (for mixture A) or Incomplete Freund's Adjuvant (for mixture B) and stirring for a night in a cold water bath. The mice were injected subcutaneously with 0.1 mL of mixture A via the tail on day 0. A booster injection of mixture B was administered on day 21. The mice were monitored at three-day intervals to track the progression of arthritis. Forty-eight male DBA/1J mice were divided into six groups, each consisting of eight mice: sham, PBS, BSA (200 ppm of BSA), BSA-BR NPs (200 ppm of BSA-BR NPs), BSA-BR-Pt NPs (200 ppm of BSA-BR-Pt NPs), and MTX (5 μg MTX in 10 μL PBS) group. Subsequent to the establishment of the CIA model, the mice were subjected to intra-articular injections of various substances in a 10 μL volume both in knee joints and ankle joints once weekly over a period of 6 weeks. After 60 days post initial immunization, the mice were euthanized and their knee joints were collected for micro-CT scanning and subsequent histological examination.

2.8. ROS scavenging activity assay and intracellular H_2O_2 assay

BMDMs were seeded in 24-well dishes with a cell density of 1×10^5 cells per well and then exposed to a combination of LPS and hypoxia (LH). After incubating the fells for 12 h, they were exposed to 200 ppm of BSA, BSA-BR NPs and BSA-BR-Pt NPs for another 12 h. Then, 10 μM of DCFH-DA from a kit for detecting reactive oxygen species (#S0033S, Beyotime Biotechnology, Shanghai, China) was introduced and allowed to incubate for 30 min. The cells were then visualized using fluorescent microscopy (Olympus).

Hydroxyl radical (•OH) assay was performed on BMDMs following the described treatment protocol. Briefly, the BBoxiProbe® Hydroxyl Radical Detection Kit (#BB-460622, BestbBio, China) was used to indicate intracellular •OH levels utilizing a specific red fluorescent probe BBoxiProbe® O28, following the manufacturer's guidelines. Subsequently, the cells were visualized using fluorescent microscopy (Olympus).

To evaluate the intracellular H_2O_2 concentration, the BBoxiProbe® Hydrogen Peroxide Detection Kit (#BB-46061, BestbBio, China) was used. BMDMs were treated with a total of 100 μM of H_2O_2 after pre-incubation with 200 ppm of BSA, BSA-BR NPs, and BSA-BR-Pt NPs for 12 h. After 1 h, the cell media was replaced with assay buffer, and the relative intracellular H_2O_2 concentration was quantified using a CLSMwith excitation/emission wavelengths of 488/525 nm.

2.9. Intracellular oxygen generation assay

To assess the level of intracellular oxygen generation in hypoxia M1 macrophages, a oxygen indicator $[Ru(dpp)_3]Cl_2$ (Alfa Aesar, Shanghai, China) was utilized following the instructions provided by the manufacturer. Briefly, hypoxic M1 macrophages were exposed to $[Ru(dpp)_3]Cl_2$ for 4 h following pre-treatment with 200 ppm of BSA, BSA-BR NPs, and BSA-BR-Pt NPs for 12 h. The fluorescence emission of $[Ru(dpp)_3]Cl_2$ (Excitation wavelength: 488 nm, Emission wavelength: 610 nm) within cells was subsequently visualized and captured using CLSM.

2.10. Cellular uptake

To confirm the cellular uptake of 5-FAM-labeled BSA-BR-Pt NPs within BMDMs, the cells were incubated with BSA-BR-Pt NPs for varying durations (2, 4, 6 h) and then analyzed by CLSM. Co-staining of the cell nucleus was achieved by using Hoechst 33342 (Thermo Fisher Scientific) for visualization in CLSM analysis.

2.11. Cell viability test

Cell viability was assessed by utilizing the Cell Counting Kit-8 (CCK-8, #C0038, Beyotime Biotechnology, Shanghai, China). Following a 12 or 24-h incubation of BMDMs with BSA, BSA-BR NPs, and BSA-BR-Pt NPs, the CCK-8 assay was carried out following the guidelines provided by the manufacturer.

2.12. HIF-1α immunostaining

HIF-1α immunostaining was conducted on BMDMs after a 12 h incubation period with LPS and hypoxia stimulation. Subsequently, the cells were treated with 200 ppm of BSA, BSA-BR NPs and BSA-BR-Pt NPs for an additional 12 h. BMDMs were immunostained with a primary antibody targeting HIF-1α (1:100, Abcam) and then with a secondary antibody labeled with Alexa Fluor 488 (1:800, Abcam). F-actin was co-stained by utilizing rhodamine phalloidin (Thermo Fisher Scientific).

2.13. Macrophage polarization phenotype and metabolic turnover test

Following the aforementioned treatment of BMDMs, the cells were fixed with 4 % paraformaldehyde and subsequently exposed to primary antibodies targeting F4/80 (1:100, Santa Cruz Biotechnology) with CD86 (1:100, Proteintech) or CD206 (1:100, Proteintech) overnight at 4 °C. Next, the cells were exposed to appropriate secondary antibodies labeled with fluorescence for an hour. DAPI (Thermo Fisher Scientific) was utilized for nuclear staining, and the specimens were visualized using a fluorescent microscope (Olympus).

ECAR and OCR are used as indicators for glycolytic and oxidative phosphorylation activities, respectively. The glycolysis assay kit (#ab197244, Abcam) and OCR plate assay kit (#E297, DOJINDO) were utilized in accordance with the manufacturer's instructions.

2.14. Quantitative reverse transcription polymerase chain reaction (qRT-PCR) and Western blot analysis

Total RNA and proteins were extracted from treated BMDMs using RNAiso Plus (TAKARA) and cell lysis buffer (Cell Signaling Technology), respectively, following the manufacturer's protocols. Subsequently, 1000 ng of RNA underwent reverse transcription with the First Strand cDNA Synthesis Kit from Thermo Fisher Scientific. SYBR green PCR Master Mix from Thermo Fisher Scientific was used with the CFX96 Connect Real-Time PCR Detection System (BIO-RAD) for qRT-PCR. The primer sequences are available in Supplementary Table S1.

For Western blot analysis, a bicinchoninic acid (BCA) kit (TherMo Fisher Scientific) was carried out for measurement of protein concentration. Following the loading of 40 μg of protein onto SDS PAGE gels, the steps of electrophoresis, membrane transfer, and sealing were carried out. Afterwards, the membranes were exposed to the primary antibodies against HIF-1α (1:1000, Abcam), NOS2 (1:1000, Proteintech), CD86 (1:1000, Proteintech), CD206 (1:1000, Proteintech), Arg-1 (1:1000, Proteintech) and β-actin (1:10000, Fudebio, Hangzhou, China), followed by a secondary antibody solution containing with horseradish peroxidase (HRP) (Fudebio, Hangzhou, China). Protein bands were identified with an ECL Kit (Fudebio, Hangzhou, China) and recorded using a gel imaging system.

2.15. Histopathological examination

The knee joints were gathered and preserved in 4 % paraformaldehyde, followed by decalcification using 15 % tetrasodium ethylenediaminetetraacetic acid for 1 months. Sections of 3 μm thickness were then prepared through paraffin embedding and stained with hematoxylin-eosin (HE), Safranin-O Fast-Green, and tartrate resistant acid phosphatase (TRAP) staining. Staining observations were conducted using a light microscope (Olympus).

2.16. Immunohistochemical (IHC) staining and analysis

A 3 μm thick section of knee joints was subjected to IHC staining with the primary antibodies directed against Hif3a (1:100, Proteintech) and Hk3 (1:100, Proteintech) according to established protocols [23], and visualized using fluorescence microscopy (Olympus). Quantitative analysis of the stained sections was conducted using ImageJ software to obtain statistical results.

2.17. μCT imaging

Before conducting histological analysis, the preserved joint samples underwent scanning with a micro-CT (Inveon Micro-CT, Siemens, Germany) at a resolution of 19 μm, 80-KV voltage, 500-μA current, and 300-ms exposure time. Subsequently, the obtained micro-CT images were examined with Materialise Mimics software (V21.0, Materialise Belgium).

2.18. Safety assessment in vivo

To assess the safety of various NPs, serum samples were obtained

from mice following treatment, and the levels of aspartate aminotransferase (AST), alanine aminotransferase (ALT), blood urea nitrogen (BUN), and creatinine (Cre) were quantified using standard kits in accordance with the manufacturer's guidelines.

2.19. RNA sequencing and analysis

BMSCs were exposed to BSA-BR-Pt NPs under hypoxia and LPS stimulation, followed by extraction of total RNA using TRIzol (TAKARA, Japan). PBS-treated BMSCs served as the control group.BGI Genomics in Shenzhen, China conducted RNA extraction, library preparation, and sequencing.SOAPnuke was used to filter the sequencing data by eliminating reads with sequencing adapters, reads with a low-quality base ratio greater than 20 % (base quality≤15), and reads with an unknown base ratio exceeding 5 %. The resulting clean reads were then saved in FASTQ format.Following analysis and data mining were conducted using the Dr. Tom Multi-omics Data mining system available at https://biosys.bgi.com.RSEM (v1.3.1) was used to determine the gene's expression level.pheatmap (v1.0.8) was used to create a heatmap based on variations in gene expression across various samples.In essence, we conducted a differential expression analysis utilizing DESeq2(v1.4.5) (or DEGseq or PoissonDis) with a Q value of ≤0.05 (or FDR of ≤0.001). Phyper conducted a Hypergeometric test to analyze the enrichment of annotated differentially expressed genes using Gene Ontology (GO) and Kyoto Encyclopedia of Genes and Genomes (KEGG) to gain insight into phenotype changes.The Q value was used to correct the significant levels of terms and pathways with a strict threshold of Q value ≤ 0.05.

2.20. Statistical analysis

The study presented quantitative results in the form of mean ± standard deviation. Statistical analysis for two-group comparisons was conducted using a Student's two-sided *t*-test, while a two-way analysis of variance (ANOVA) was employed for multiple comparisons. Statistical significance was defined as a *P*-value <0.05.

3. Results and discussion

3.1. Preparation of BSA-BR-Pt NPs

As illustrated in Scheme1, the BSA-BR NPs were prepared by a facile hydrophilic-hydrophobic interaction followed by Pt NPs loading. Through transmission electron microscopy (TEM) observation, the BSA-BR NPs presented a spherical shape with good dispersity (Fig. 1A). The loading content and loading efficiency of BR were determined to be 1.12 % and 28.02 %, respectively, through its standard curve (Fig. S1). After Pt loading, the size of BSA-BR-Pt NPs was approximately 395.9 ± 52.3 nm (Fig. 1B). The successful loading of Pt was evidenced through the energy disperse spectroscopy observation (Fig. S2). The Pt loading content was calculated to be 0.918 % through the inductively coupled plasma optical emission spectrometry (ICP-OES) measurement. These BSA-BR-Pt NPs displayed desirable reproducibility with negligible difference between all batches. The hydrodynamic size of BSA-BR NPs and BSA-BR-Pt NPs was measured to be 344.9 ± 11.3 nm and 375.9 ± 24.5 nm, respectively (Fig. 1C–E). The surface charge of BSA-BR NPs was around −13.0 ± 2.4 mV, which changed to −15.3 ± 1.4 mV after Pt loading (Fig. 1F). UV–Vis–NIR spectra revealed that a characteristic absorption peak of pure BR was observed around 450 nm, which exhibited a slight redshift in BSA-BR and BSA-BR-Pt NPs (Fig. 1G). The broad peak in BSA-BR-Pt NPs could be attributed to the formation of Pt NPs. Fourier transform infrared (FTIR) spectra revealed that BR exhibited N–H bending vibration at 3413.83 cm^{-1}, the C=O stretching vibration at 1688.82 cm^{-1}, and the C=C stretching vibration at 1641.28 cm^{-1}, which closely resembled the spectra of BSA-BR and BSA-BR-Pt NPs (Fig. 1H). The intensified absorption around 3400 cm^{-1} could be caused by the presence of BSA which enriched with O–H. The color of the BSA-BR-Pt NPs underwent a slight darkening when compared to BSA-BR NPs, indicating the successful incorporation of Pt nanoparticles (Fig. S3). All these findings collectively demonstrate the successful preparation of BSA-BR-Pt NPs.

Then, the anti-inflammatory capacity of BSA-BR NPs was examined by utilizing Cu^{+} and H_2O_2 as the source of hydroxyl radical (•OH) and MB as the probe. The absorption peak of MB could be decreased in the presence of •OH. The absence of BSA-BR NPs in the control experiment led to a gradual decrease in the peak of MB over time, suggesting the

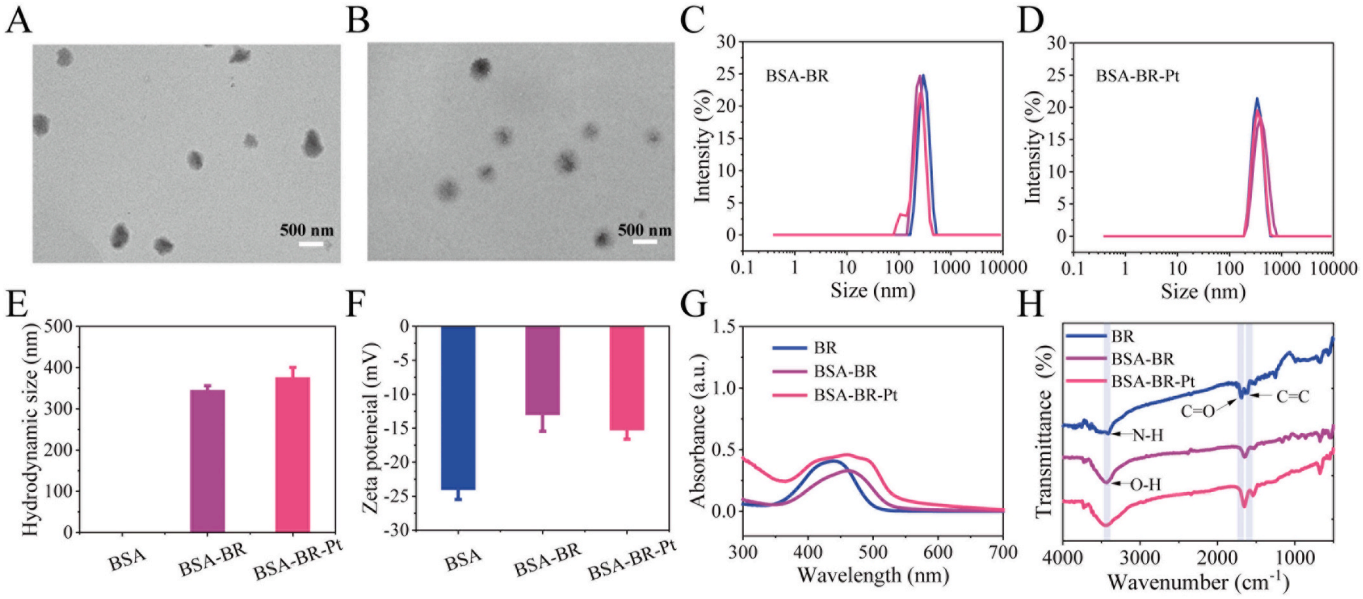

Fig. 1. Preparation and characterization of BSA-BR-Pt NPs. **(A, B)** TEM images of BSA-BR NPs (A) and BSA-BR-Pt NPs (B). **(C, D)** Hydrodynamic sizes of BSA-BR NPs (C) and BSA-BR-Pt NPs (D). n = 3 per group. **(E, F)** Hydrodynamic sizes (E) and zeta potential (F) of BSA, BSA-BR NPs, and BSA-BR-Pt NPs. **(G, H)** UV–Vis absorption spectra (G) and FTIR spectra (H) of BR, BSA-BR NPs, and BSA-BR-Pt NPs.

production of •OH in the mixture (Fig. 2A–E). In the presence of BSA-BR NPs, the decrease of MB peak was compromised with the increase of NP concentration and reaction time (Fig. 2F). The change in MB content was also proved by the digital photos of the solution after different reactions (Fig. S4). Subsequently, the clearance capacity of H_2O_2 was investigated when mixed with BSA-BR NPs and BSA-BR-Pt NPs of varying concentrations and shaking for 1 h at 37 °C, (Fig. 2G and Fig. S5). It was observed that the H_2O_2 level decreased with the increase in the concentration of BSA-BR NPs, indicating the H_2O_2 clearance ability of BSA-BR NPs. The concentration of H_2O_2 decreased more quickly in the presence of BSA-BR-Pt NPs, indicating the synergistic effect of BR and Pt on H_2O_2 scavenging. Oxygen generation experiments were used to assess the catalase-like function of Pt nanoparticles (Fig. 2H). As shown in Fig. 2H, O_2 levels gradually increased with the increase in the concentration of BSA-BR-Pt NPs and reaction time, proving that Pt could catalyze H_2O_2 into O_2 effectively.

3.2. Hypoxia improvement and ROS scavenging of BSA-BR-Pt NPs in vitro

Subsequently, we performed *in vitro* experiments using bone marrow-derived macrophages (BMDMs) obtained from mice. Following incubation with 5-FAM-labeled BSA-BR-Pt NPs, confocal laser scanning microscopy (CLSM) revealed significant cellular internalization of BSA-BR-Pt NPs by BMDMs in a manner dependent on both time and concentration (Fig. 3A, B and Fig. S6). The results of Calcein-AM and propidium iodide (AM/PI) staining and CCK-8 assay indicated that 200 ppm BSA, BSA-BR NPs, and BSA-BR-Pt NPs did not exhibit cytotoxicity within a 12 and 24 h period. However, when concentration exceeded 400 ppm, BSA-BR-Pt NPs demonstrated a mild cytotoxic effect, with the degree of cytotoxicity escalating in correlation with concentration levels (Fig. 3C, D and Fig. S7 and S8). Consequently, subsequent *in vitro* experiments were conducted using a concentration of 200 ppm BSA-BR-Pt NPs.

The production of oxygen in hypoxic M1 macrophages via the catalysis of various NPs was first investigated. BMDMs were treated with BSA, BSA-BR NPs and BSA-BR-Pt NPs under hypoxic and inflammatory conditions induced by a hypoxic atmosphere and 500 ng/mL lipopolysaccharide (LPS). Fluorescence intensity (red) of the oxygen probe [Ru(dpp)3]Cl2 was significantly diminished in hypoxia M1 BMDMs treated with BSA-BR-Pt NPs, suggesting a substantial increase in intracellular oxygen generation. Conversely, the fluorescent signal remained relatively stable when nanoparticles lacking Pt were used (Fig. 3E and F). To further assess the efficacy of BSA-BR-Pt NPs in mitigating hypoxia, we evaluated HIF-1α cellular localization and expression levels. The combination of LPS and hypoxia (LH) stimulation resulted in a notable increase in the translocation of HIF-1α from the cytoplasm to the nucleus, along with a significant upregulation of HIF-1α expression level. BSA-BR-Pt NPs treatment effectively reduced the expression of HIF-1α and its nuclear translocation in hypoxic M1 macrophages. The role of this treatment exceeded that of BSA-BR NPs treatment (Fig. 3G, H, 5E and F). Although BSA-BR NPs did not generate oxygen, our findings demonstrated that BSA-BR NPs could still improve hypoxia partially through inhibiting the expression of HIF-1α and its nuclear translocation, which complemented the additional function of bilirubin NPs as antioxidants [18,24]. These results demonstrated that the incorporation of platinum with oxygen-generating property into BSA-BR NPs, suppressed the expression of HIF-1α and its nuclear translocation in hypoxic M1 macrophages through a synergistic mechanism.

To evaluate the ROS scavenging effect of BSA-BR-Pt NPs in hypoxic M1 macrophages, the 2′-7′-dichlorodihydrofluorescein diacetate (DCFH-DA) was used as a fluorescent probe to measure the overall intracellular ROS levels. Hypoxic M1 macrophages exhibited elevated levels of ROS, as indicated by the intense fluorescence emission. After treatment with BR-Pt NPs or BSA-BR-Pt NPs, the ROS level markedly decreased in hypoxic M1 macrophages (Fig. 4A and B). Notably, BSA-BR-Pt NPs demonstrated superior efficacy in the scavenging of ROS in comparison to BSA-BR NPs. The observed trend of •OH fluorescent probe was consistent with this result, showing a decrease of intracellular •OH levels in hypoxic M1 macrophages with BSA-BR-Pt NPs treatment (Fig. 4C and D). Intracellular H_2O_2 levels were then evaluated utilizing an intracellular H_2O_2 assay kit. Following pretreatment with BSA, BSA-BR NPs, and BSA-BR-Pt NPs, BMDMs were exposed to 100 μM H_2O_2 for 1 h, and intracellular H_2O_2 levels were quantified based on fluorescence

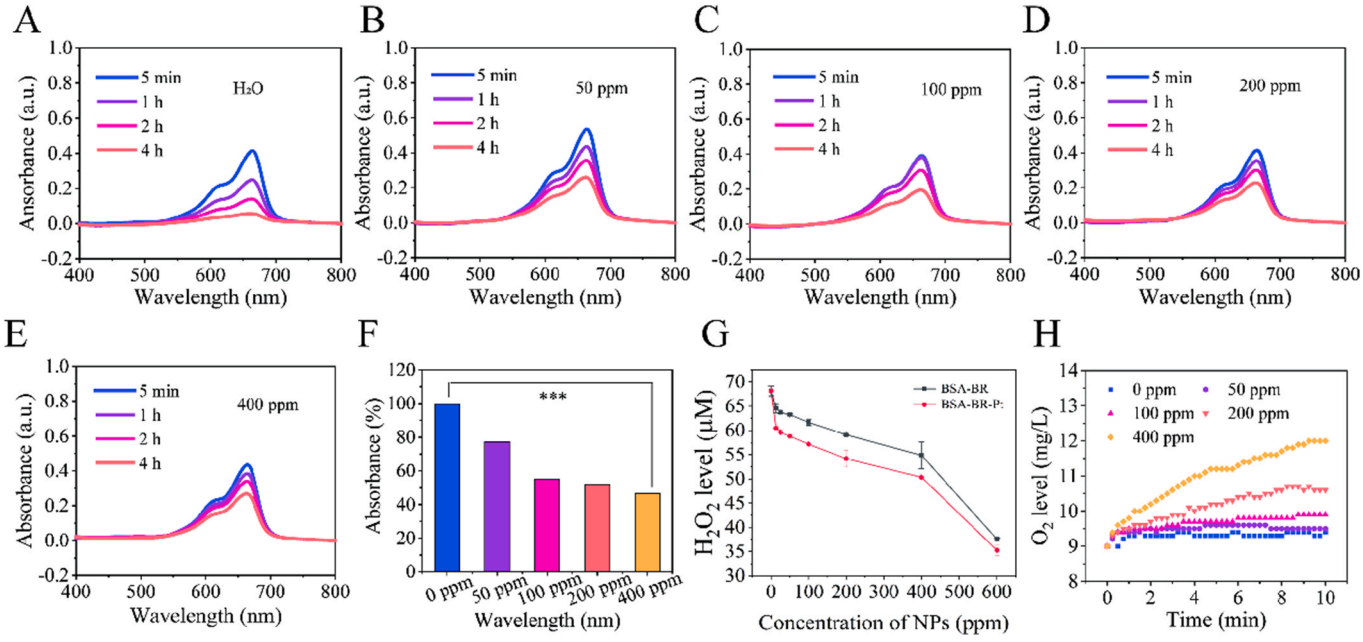

Fig. 2. ROS scavenging and O_2 generation by BSA-BR NPs and BSA-BR-Pt NPs. **(A–E)** UV–Vis spectra of MB for •OH level detection with (A) 0 ppm, (B) 50 ppm, (C) 100 ppm, (D) 200 ppm, and (E) 400 ppm of BSA-BR NPs. **(F)** The relative intensity decrease of MB absorption peak in the presence of BSA-BR NPs with different concentrations after 4 h reaction. **(G)** H_2O_2 level detection in the presence of BSA-BR NPs and BSA-BR-Pt NPs with different concentrations. **(H)** O_2 production detection in the presence of BSA-BR-Pt NPs with different concentrations.

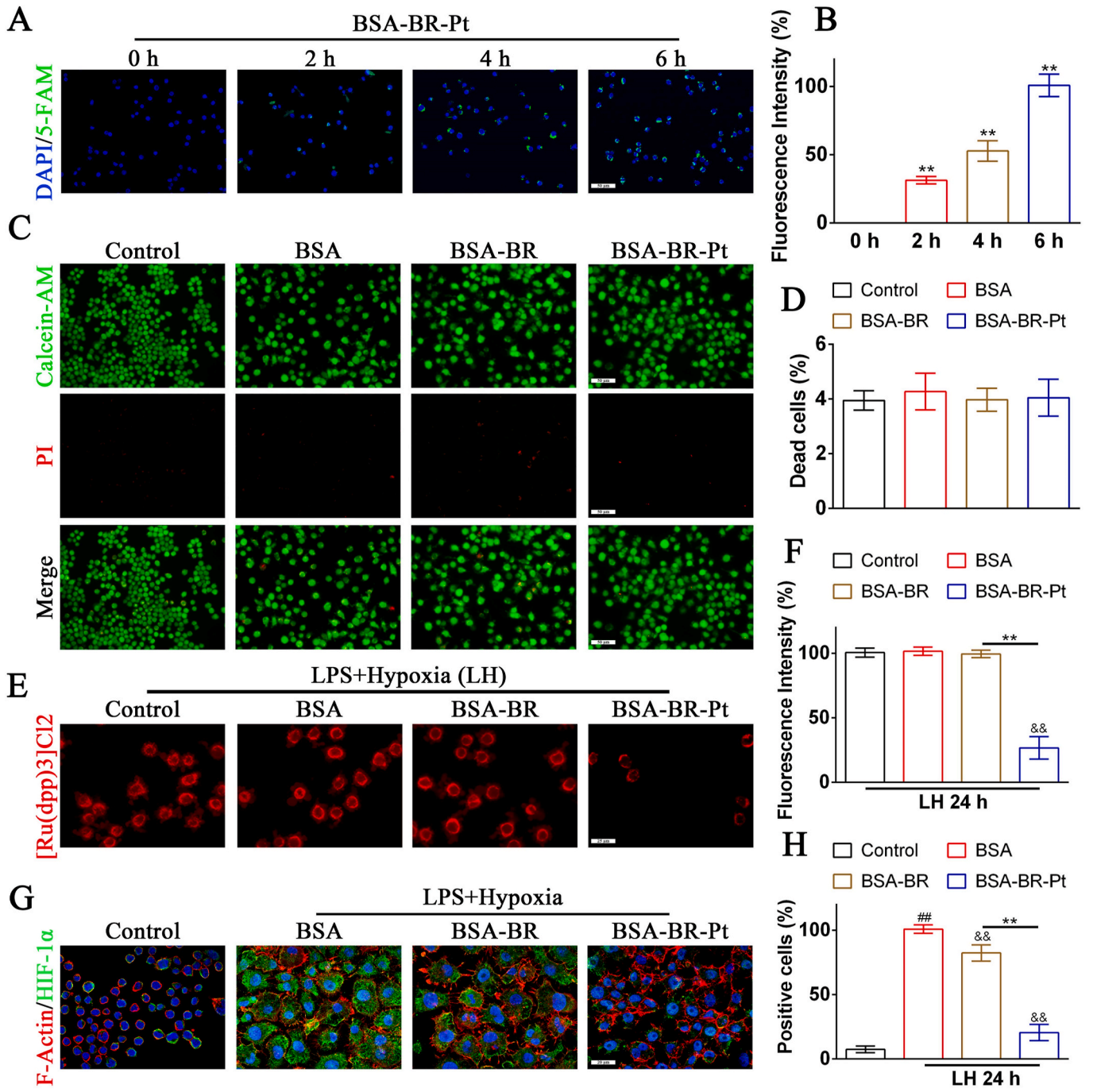

Fig. 3. The decrease of HIF-1α levels and O2 generation in hypoxic M1 macrophages treated with BSA-BR-Pt NPs. **(A, B)** Representative CLSM images and relative fluorescence intensity of BSA-BR-Pt NPs internalized by BMDMs following 5-FAM labeling. Scale bar: 50 μm. **(C, D)** Representative fluorescence images and quantification of various treatments on BMDMs stained with Calcein-AM/PI. Green and red represent live and dead cells respectively. Scale bar: 50 μm. **(E, F)** Representative CLSM images and relative fluorescence intensity of the oxygen indicator [Ru(dpp)3]Cl2 in BMDMs with various treatment. The red fluorescence emitted by the dye was attenuated in the presence of oxygen. LH indicates LPS and hypoxia. Scale bar: 25 μm. **(G, H)** Representative CLSM images and quantification of various treatments of BMDMs stained with HIF-1α and F-Actin. Scale bar: 20 μm. Normoxia as the control group. #, & and * indicate significant differences when compared with the control, LH + BSA and LH + BSA-BR-Pt NPs, respectively (##, &&, $^{**}P < 0.01$).

intensity. The intracellular decomposition of H_2O_2 by BSA-BR-Pt NPs was found to be more efficient than that of control groups, as demonstrated in Fig. 4E and F. This observation aligns with earlier findings presented in Fig. 2G, indicating the synergistic H_2O_2-degrading capacity of BSA-BR-Pt NPs. These data also demonstrated the advantage of BSA-BR-Pt NPs due to the synergistic effect of BR and Pt on ROS scavenging. Collectively, these findings indicated that the addition of platinum with hypoxia-attenuating property to BSA-BR NPs enhanced ROS elimination in hypoxic M1 macrophages via a synergistic mechanism.

3.3. *BSA-BR-Pt NPs reprogram M1 macrophages toward M2 macrophages in vitro*

Synovial hypoxia increased the expression of HIF-1α and promoted excessive ROS generation, resulting in augmented polarization of pro-inflammatory M1 macrophages and diminished polarization of anti-

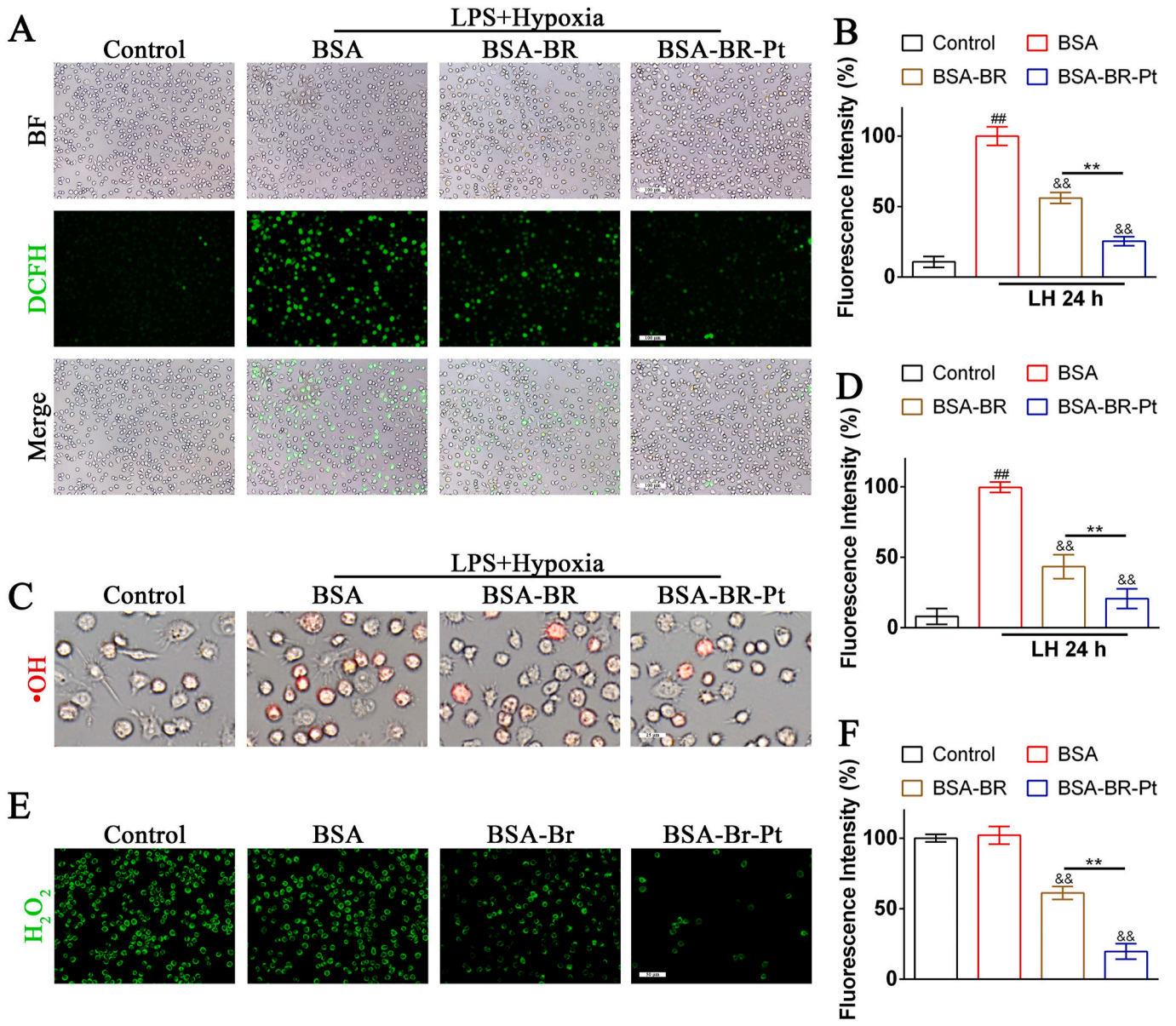

Fig. 4. ROS scavenging of BSA-BR-Pt NPs in hypoxic M1 macrophages. **(A, B)** Representative fluorescence images and relative fluorescence intensity of various treatments of BMDMs stained with ROS fluorescent probe DCFH-DA. LH indicates LPS and hypoxia. Scale bar: 100 μm. **(C, D)** Representative fluorescence images and relative fluorescence intensity of various treatments of BMDMs stained with •OH fluorescent probe. Scale bar: 25 μm. **(E, F)** Representative CLSM images and relative fluorescence intensity of intracellular H_2O_2 in BMDMs with various treatment. Scale bar: 50 μm #, & and * indicate significant differences when compared with the control, LH + BSA and LH + BSA-BR-Pt NPs, respectively (##, &&, $^{**}P < 0.01$).

inflammatory M2 macrophages in the RA joints [25,26]. A prominent characteristic of hypoxic M1 macrophages was their heightened ability for proliferation [8]. Consequently, a CCK-8 assay was conducted to evaluate the effect of BSA-BR-Pt NPs on the proliferation of M1 macrophages. The results from CCK-8 assay showed that the enhanced proliferation of M1 macrophages was significantly inhibited after BSA-BR-Pt NPs treatment under both normoxic and hypoxic conditions (Fig. S9). Based on the observed capacity of BSA-BR-Pt NPs to efficiently suppress HIF-1α expression and reduce ROS production in hypoxic M1 macrophages, we postulated that the NPs might induce a phenotypic shift from M1 to M2 macrophages.

To investigate this postulation, we next conducted an *in vitro* assessment of the transition from M1 to M2 phenotype in BMDMs after exposure to BSA-BR-Pt NPs under conditions of hypoxia and LPS stimulation. These cells were then subjected to immunofluorescence staining for F4/80 (a macrophage marker) with CD86 (an M1 marker) or CD206 (an M2 marker). Our findings revealed a significant upregulation of CD86 and a noticeable downregulation of CD206 in BMDMs exposed to hypoxia and LPS. After treatment of BSA-BR-Pt NPs, there was a reduction in the fluorescence intensity of CD86 and an increase in the fluorescence intensity of CD206, indicating a potential re-polarization of macrophages from M1 macrophages to M2 macrophages (Fig. 5A–D). Moreover, Western blot analysis demonstrated that a notable rise in the protein level of markers for M1 macrophages markers, such as NOS2 and CD86, and a substantial decline in the protein level of markers for M2 macrophages markers, including CD206 and arginase-1 (Arg-1), following hypoxia and LPS stimulation. Consistent with expectations, downregulated expression of M1 macrophages markers and upregulated expression of M2 macrophages markers were observed in hypoxic M1 macrophages with BSA-BR-Pt NPs treatment (Fig. 5E). Similarly, qRT-PCR analysis revealed that hypoxia and LPS treatment significantly increased mRNA expression levels of NOS2, CD86, IL-1β and TNF-α, and

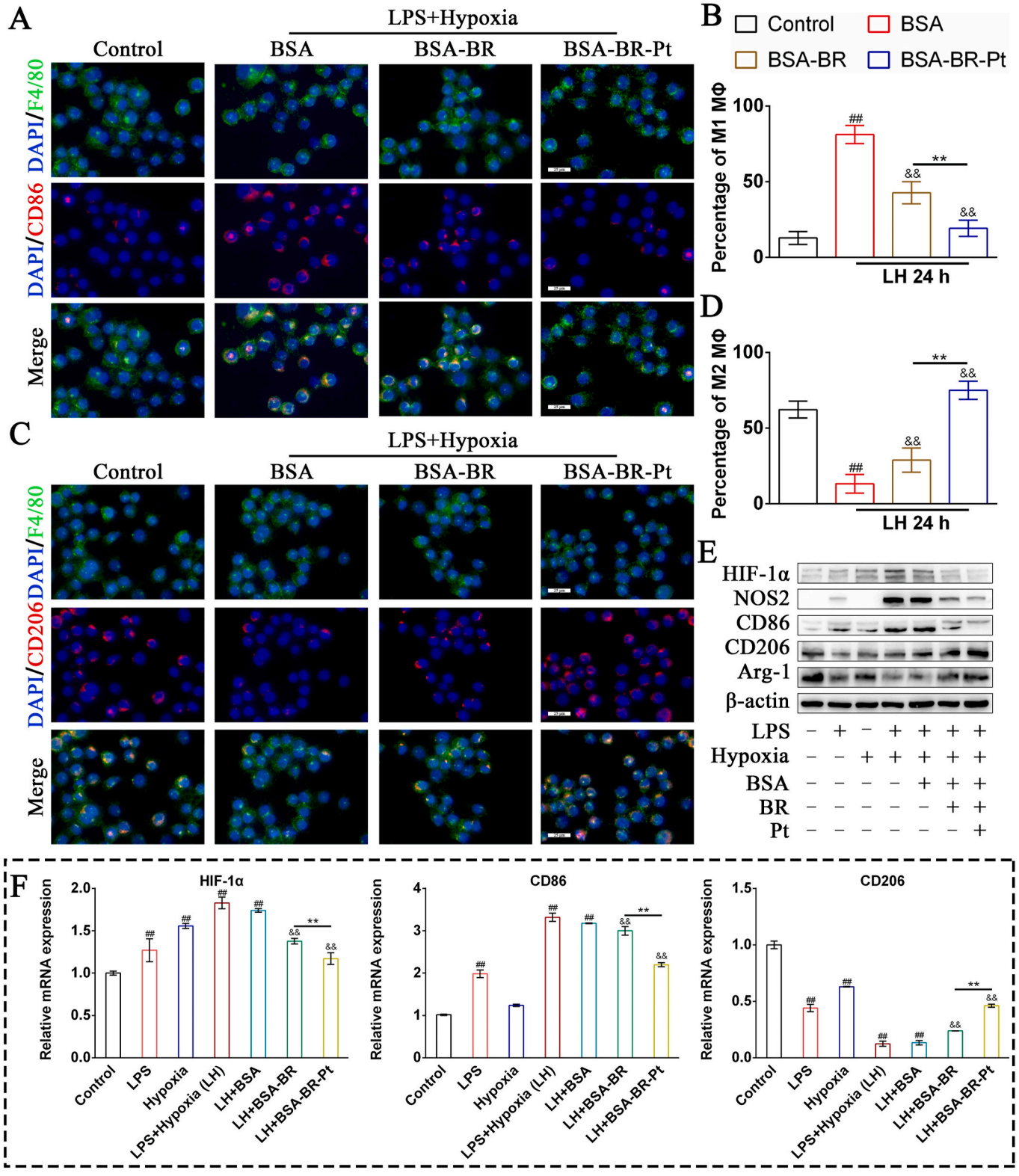

Fig. 5. BSA-BR-Pt NPs reprogram M1 polarized macrophages to M2 polarized macrophages. **(A–D)** Representative immunofluorescence staining and quantification of F4/80 (green) with CD86 (red) (A and B) or CD206 (red) (C and D), and nuclei (blue) on BMDMs treated with different treatment. Scale bar: 25 μm. **(E)** Immunoblot analysis of HIF-1α, NOS2, CD86, CD206, and Arg-1 in different treated-BMDMs. **(F)** qRT-PCR analysis of HIF-1α, CD86, and CD206 mRNA expression in BMDMs with various treatment. #, & and * indicate significant differences when compared with the control, LH + BSA and LH + BSA-BR-Pt NPs, respectively (##, &&, $^{**}P < 0.01$).

reduced mRNA expression levels of Arg-1, CD206, IL-4 and IL-10. Notably, treatment with BSA-BR-Pt NPs markedly reduced mRNA expression levels of NOS2, CD86, IL-1β, IL-6 and TNF-α, and elevated mRNA expression levels of Arg-1, CD206, IL-4 and IL-10 (Fig. 5F and Fig. S10). BSA-BR NPs also showed a macrophage reprogramming effect but to a lesser extent than that of BSA-BR-Pt NPs. The consistent trend observed in the M1 markers and HIF-1α expression indicates a vital role for HIF-1α in the activation of M1 polarized macrophages [27,28]. The significantly decreased expression of HIF-1α in the BSA-BR-Pt NPs group compared to the BSA-BR NPs group suggests that the superior macrophage reprogramming effect in the former group is likely facilitated by suppressing HIF-1α (Fig. 5E and F and Fig. S10). Collectively, we confirmed the successful transition of macrophages from M1 to M2 phenotype induced by BSA-BR-Pt NPs via synergistic improvement of hypoxia and elimination of ROS.

3.4. BSA-BR-Pt NPs attenuate the progression of RA in CIA mice

The therapeutic efficacy of BSA-BR-Pt NPs treatment was subsequently assessed in CIA mice, a model widely recognized for its systemic immune responses in experimental RA research (Fig. 6A). Methotrexate (MTX), a commonly used small-molecule disease-modifying antirheumatic drug DMARD, was employed as the positive control group. In comparison to the PBS-treated mice, those administered with BSA-BR

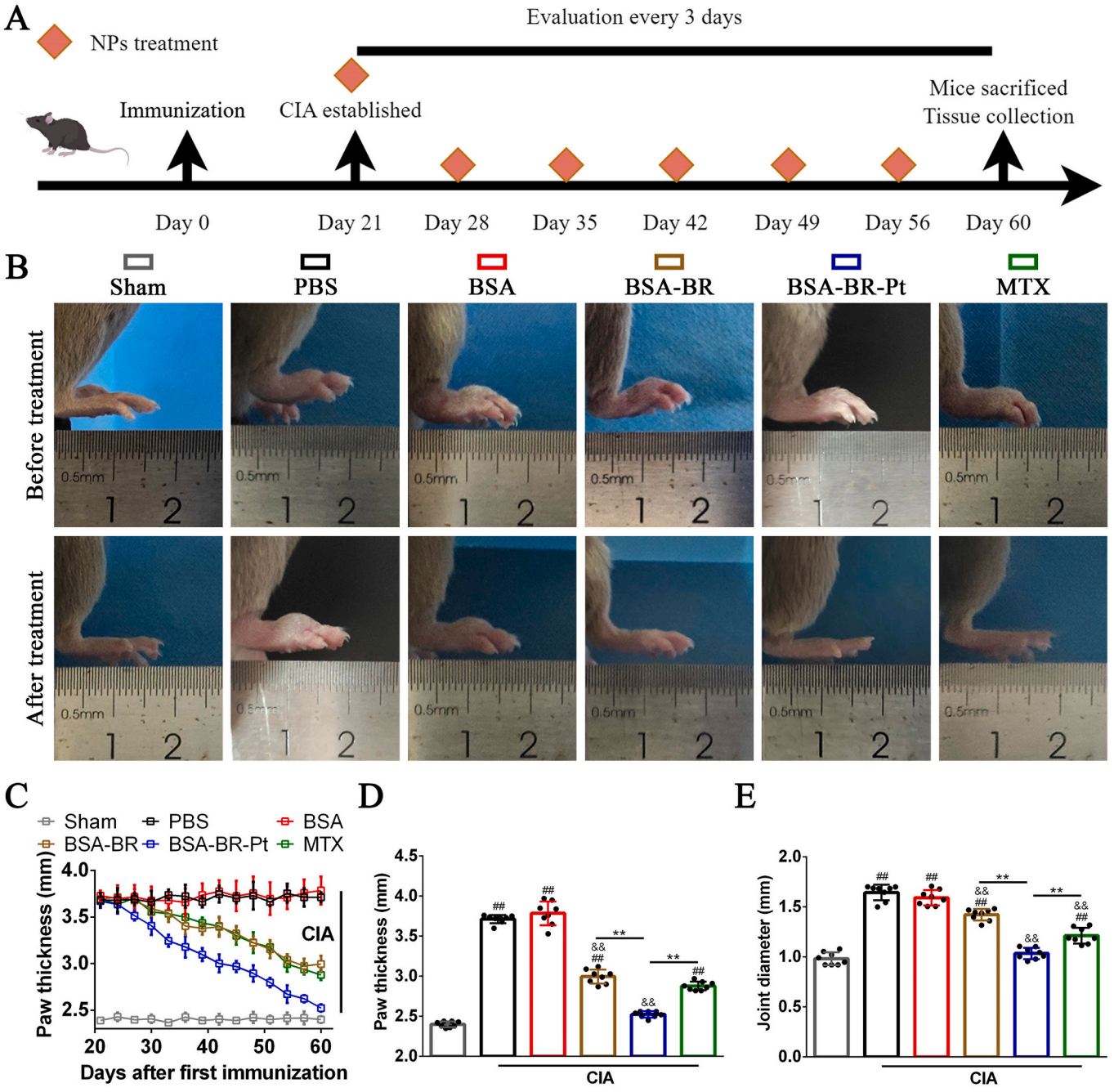

Fig. 6. Therapeutic effect of BSA-BR-Pt NPs in CIA mice. **(A)** The schematic illustration of BSA-BR-Pt NPs treatment. **(B)** Representative photographs of joints in CIA mice before and after different treatment. **(C)** Inflammatory joint paw thickness over time for various treatments. **(D, E)** The statistic result of paw thickness (D) and joint diameter (E) between different treatments at day 60 following immunization. #, & and * indicate significant differences when compared with the sham, PBS, and BSA-BR-Pt NPs groups, respectively (##, &&, $^{**}P < 0.01$).

NPs, BSA-BR-Pt NPs or MTX exhibited obvious improvement in the degree of swelling. Although mice treated with BSA displayed no therapeutic effect, the BSA-BR NPs, BSA-BR-Pt NPs, and MTX notably reduced paw thickness and joint diameter compared to PBS group. Specifically, treatment with BSA-BR-Pt NPs demonstrated great effects, resulting in 43 % and 42 % decrease in paw thickness and knee joint diameter, respectively, compared to treatment with MTX (Fig. 6B–E). To further evaluate the extent of joint inflammation and cartilage destruction, histological examination of the knee and ankle joint slides from mice was performed. H&E stained sections in the knee and ankle joints from CIA mice treated with PBS or BSA showed a notable presence of inflammatory cell infiltration and severe synovial hyperplasia. The BSA-BR NPs and MTX groups demonstrated a similar reduction in synovial inflammation and synovitis score. Importantly, treatment with BSA-BR-Pt NPs showed superior efficacy in attenuating synovitis in the knee and ankle joints compared to the other groups (Fig. 7A–D). As the BSA-BR-Pt NPs were found to significantly induce a phenotypic transition from M1 to M2 macrophages *in vitro*, our subsequent investigation involved the identification of macrophage subtypes in synovial tissue through the examination of the colocalization of F4/80 with CD86 or CD206 (Fig. 7E–H and Fig. S11). As expected, the BSA-BR-Pt NPs group exhibited a significant transition from M1 to M2 polarization in the knee and ankle joints, resulting in superior efficacy in combating synovitis compared to the other groups. Safranin-O Fast-Green staining and H&E staining showed a marked depletion of cartilage tissues in the knee and ankle joints of the PBS and BSA groups. In sharp contrast, the knee and ankle joints of the BSA-BR-Pt NPs and MTX groups displayed intact and red-stained cartilage, indicating that BSA-BR-Pt NPs effectively mitigated articular cartilage lesions. Concretely, administration with BSA-BR-Pt NPs exhibited superior effects, leading to a 45 % decrease in synovitis score and a 35 % decrease in Mankin score in the knee joint, as well as a 32 % reduction in synovistis score and a 48 % reduction in Mankin score in the ankle joint, when compared to administration with MTX (Fig. 7A–D, Fig. 8A, B, G, H and Fig. S12A and C)

Bone erosion was considered as a pathology associated with late-stage RA [29]. In order to assess the potential of BSA-BR-Pt NPs to mitigate inflammatory bone resorption, we evaluated the impacts of BSA-BR-Pt NPs on the expression levels of osteoclasts markers through tartrate-resistant acid phosphatase (TRAP) staining. TRAP-positive multinuclear cells with more than three nuclei were identified as osteoclasts. The presence of elevated osteoclasts was observed in the regions of bone erosion and subchondral bone in the PBS and BSA groups. While BSA-BR NPs and MTX treatments resulted in a comparable decrease in osteoclast numbers, treatment with BSA-BR-Pt NPs exhibited superior efficacy in reducing osteoclast numbers in the knee and ankle joints (Fig. 8C, D, I, J and Fig. S12B and D). Micro-CT analysis provided additional confirmation of bone erosion in a more detailed manner. The knee and ankle joints exhibited obvious bone damage in the PBS and BSA groups, with BSA-BR NPs, BSA-BR-Pt NPs and MTX treatment demonstrating a noticeable alleviation of bone destruction compared to the PBS groups. It is noteworthy that the superior therapeutic effect was found in the BSA-BR-Pt NPs group compared to the BSA-BR NPs and MTX groups. To be specific, BSA-BR-Pt NPs administration showed significant efficacy, resulting in a 58 % and 63 % decrease in the knee and ankle joints of bone erosion area compared to MTX administration (Fig. 8E, F, K, and L). The data provided above support that BSA-BR-Pt NPs could effectively mitigate the development of RA by attenuating synovial inflammation, cartilage damage and bone erosion in CIA mice.

In consideration of safety, hepatotoxicity was assessed through the measurement of serum levels of liver enzymes alanine transaminase (ALT) and aspartate aminotransferase (AST) following treatment (Figs. S13A and B), while nephrotoxicity was evaluated by measuring blood urea nitrogen (BUN) and creatinine (Cre) (Figs. S13C and D). The results indicated that there were no significant changes in these parameters after treatment with PBS, BSA, BSA-BR NPs, BSA-BR-Pt NPs, or MTX compared to the sham mice, suggesting minimal toxicity to the liver and kidney. Although the intra-articular injection of MTX did not lead to abnormal alterations in ALT, AST, BUN, and Cre indices, Yang et al. observed that intravenous administration of MTX led to a notable increase in AST and Cre levels in mice, potentially indicating hepatic and renal damage following prolonged intravenous use [14,28]. This highlights the constraints of MTX in clinical practice due to its adverse effects. Taken together, these findings suggested that intra-articular injection of BSA-BR-Pt NPs with improved efficacy and safety profiles may present a more favorable option for RA treatment.

3.5. *The functional mechanism of BSA-BR-Pt NPs on macrophages reprogramming and RA therapy*

In order to elucidate the underlying mechanism of BSA-BR-Pt NPs treatment on macrophage reprogramming in the development of RA, macrophages treated with either PBS (LH_Ctrl) or BSA-BR-Pt NPs (LH_BBP) were harvested after hypoxia and LPS stimulation for bulk-RNA sequencing analysis. A total of 1117 differentially expressed genes (DEGs) were detected in the comparison between LH_BBP and LH_Ctrl, including 195 identically downregulated genes and 992 identically upregulated genes (Fig. 9A, B and Fig. S14 and Table S2). Gene Ontology (GO) and Kyoto Encyclopedia of Genes and Genomes (KEGG) enrichment analysis were utilized to annotate the functions of these genes. The findings from the Go analysis (Fig. 9C and Fig. S15A) indicated that the identified genes primarily participate in various biological processes, such as immune system process, metabolic process, inflammatory response, cellular response to LPS, angiogenesis, positive regulation of angiogenesis, cellular response to hypoxia, and response to hypoxia, which were associated with the progression of RA [9,12,25,30–32]. As BSA-BR-Pt NPs with synergistic hypoxia improvement and ROS scavenging, we focus on DEGs in cellular response to hypoxia and response to hypoxia between LH_BBP and LH_Ctrl. Cluster analysis revealed that a number of DEGs linked to hypoxia in the LH_BBP group were downregulated, such as Hif3a, Egln3, Vegfa, Hmox1 and Ptgis (Fig. 9D and E). These findings were further corroborated through qRT-PCR in hypoxic M1 macrophages treated with PBS or BSA-BR-Pt NPs. Compared to the control group, a reduction in mRNA expression levels of Hif3a, Egln3, Vegfa, Hmox1 and Ptgis were observed in the LH_BBP group (Fig. 9F and Fig. S16). Results from immunohistochemistry (IHC) staining indicated a marked increase in Hif3a positive cells within the synovium of CIA mice compared to the sham group. BSA-BR NPs and MTX effectively reduced the expression of Hif3a in hypoxic synovium, whereas the therapeutic efficacy of these treatments were found to be less pronounced compared to that of BSA-BR-Pt NPs (Fig. 9G and H), which were consistent with attenuating RA progression, as depicted in Figs. 6–8. HIF-1α, HIF-2α, and HIF-3α (Hif3a), which are part of the hypoxia-inducible factors-α, have been identified as crucial controllers of the adaptive reaction to alterations in oxygen concentration [33,34]. While the roles and mechanisms of HIF-1α and HIF-2α in response to low oxygen levels had been extensively studied across various disciplines [32,35], research on the function of Hif3a in hypoxic condition was notably scarce. Our study revealed Hif3a as a novel target within the enzyme-catalyzed nanoplatform for orchestrating the reprogramming of hypoxic M1 macrophage polarization. Furthermore, analysis using Go annotations (Fig. S15A, S17A and B) suggested that the identified genes were predominantly involved in a variety of molecular functions (such as catalytic activity, molecular function regulator, and antioxidant activity), as well as cellular component (such as extracellular space, and cytoplasm). This demonstrates BSA-BR-Pt NPs possess both catalytic and antioxidant properties, which play a crucial role on modulating cellular molecular functions and contributing to extracellular interactions.

In addition, the upregulation of Vegfa, a proangiogenic cytokine, in hypoxic M1 macrophages promoted the recruitment of inflammatory cells and their cytokines, leading to persistent synovitis in RA [32,36]. The administration of BSA-BR-Pt NPs had been shown to inhibit the

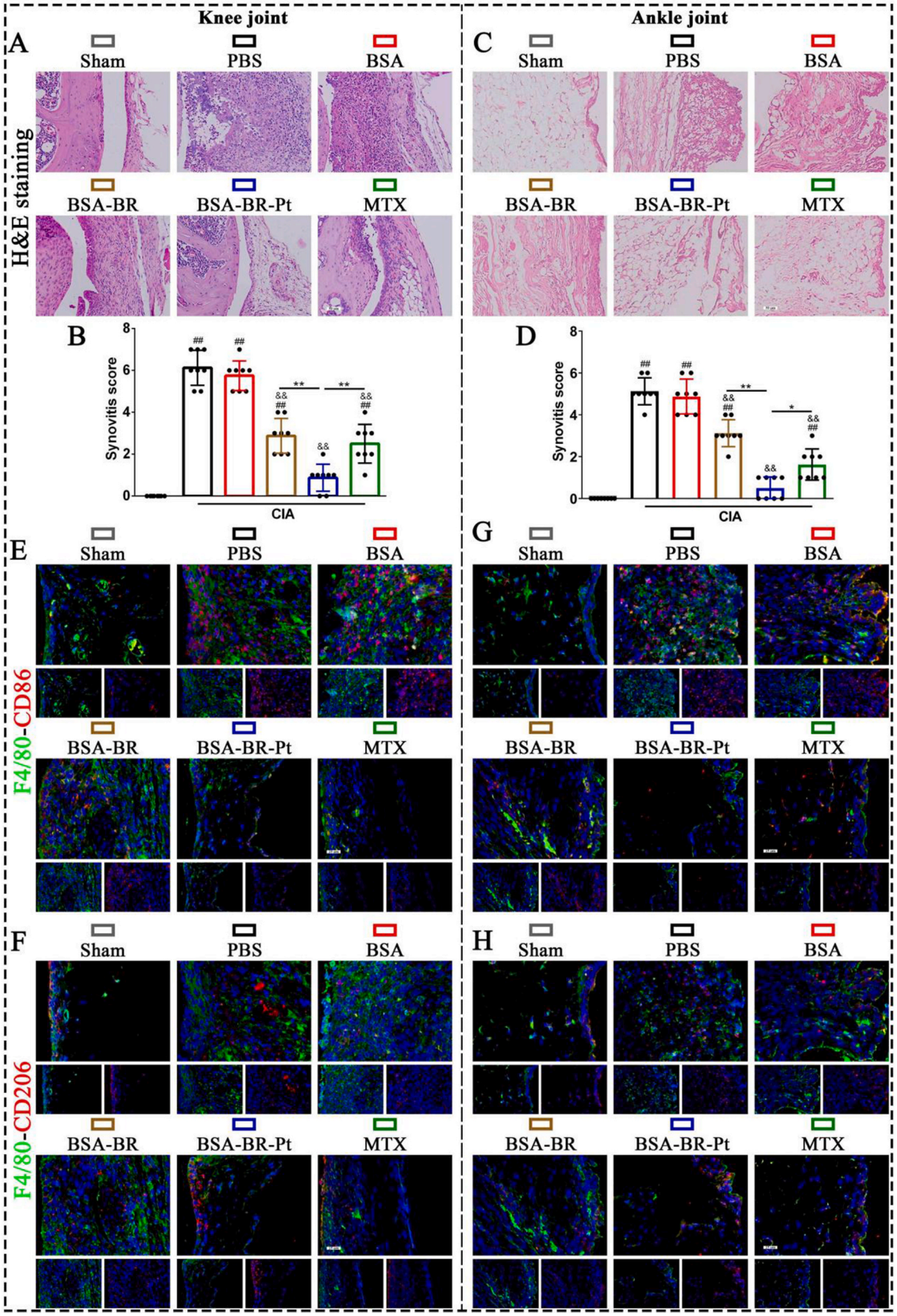

Fig. 7. Treatment of BSA-BR-Pt NPs attenuates synovitis and reprograms macrophage polarization in CIA mice. **(A–D)** Representative images and quantified analysis of H&E staining in the knee and ankle joints of CIA mice with different treatment. Scale bar: 50 μm. **(E–H)** Representative images of coimmunostaining of F4/80 with CD86 or CD206 in the knee and ankle joints of CIA mice with different treatment. Scale bar: 25 μm #, & and * indicate significant differences when compared with the sham, PBS, and BSA-BR-Pt NPs groups, respectively (*P < 0.05 and ##, &&, **P < 0.01).

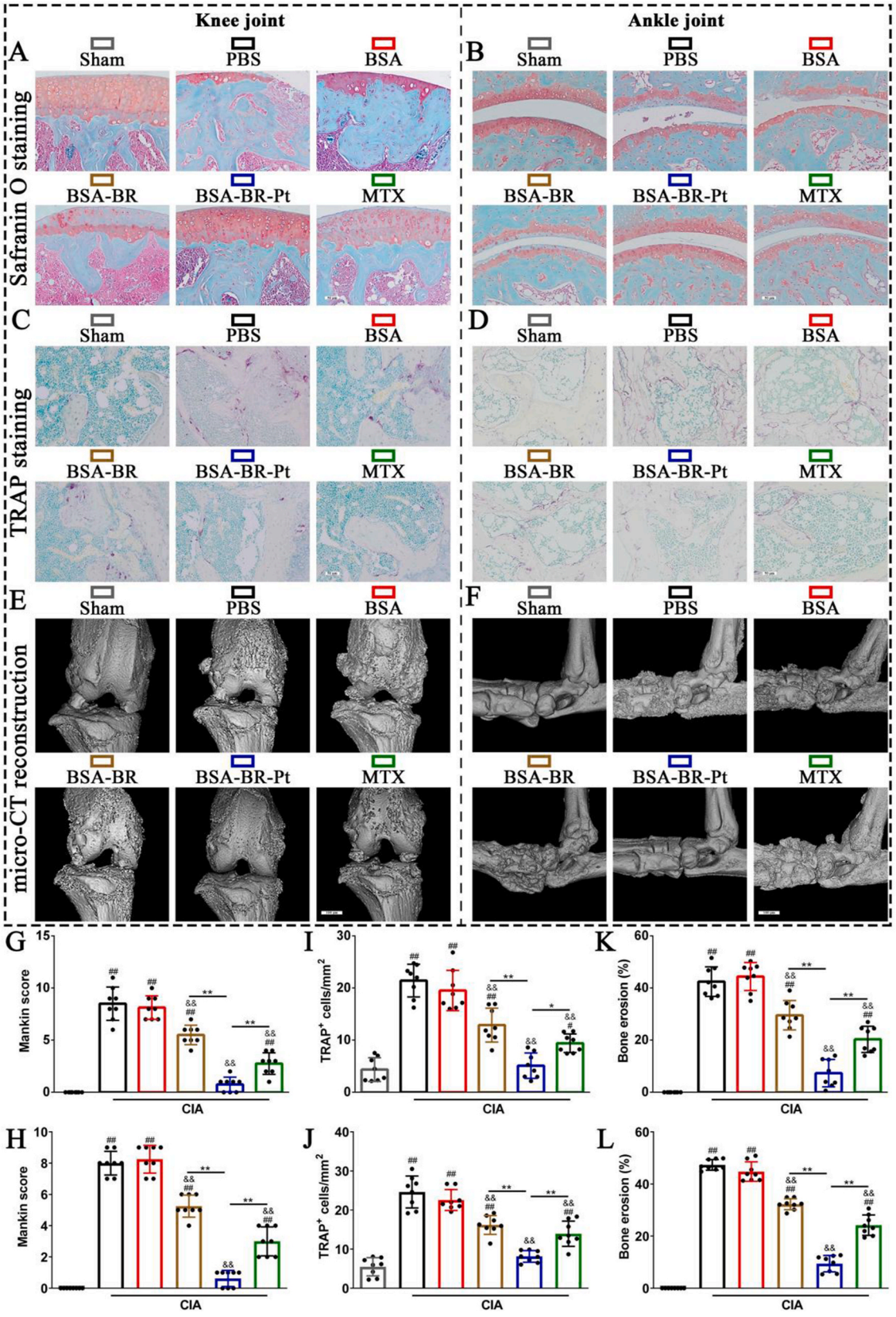

Fig. 8. Treatment of BSA-BR-Pt NPs mitigates cartilage degeneration and bone erosion in CIA mice. **(A–L)** Representative images and quantified analysis of safranin O and fast green staining (A and B), TRAP staining (C and D) and micro-CT (E and F) in the knee (G–K) and ankle (H–L) joints of CIA mice with different treatment. Scale bar: 50 μm and 100 μm #, & and * indicate significant differences when compared with the sham, PBS, and BSA-BR-Pt NPs groups, respectively (*P < 0.05 and ##, &&, **P < 0.01).

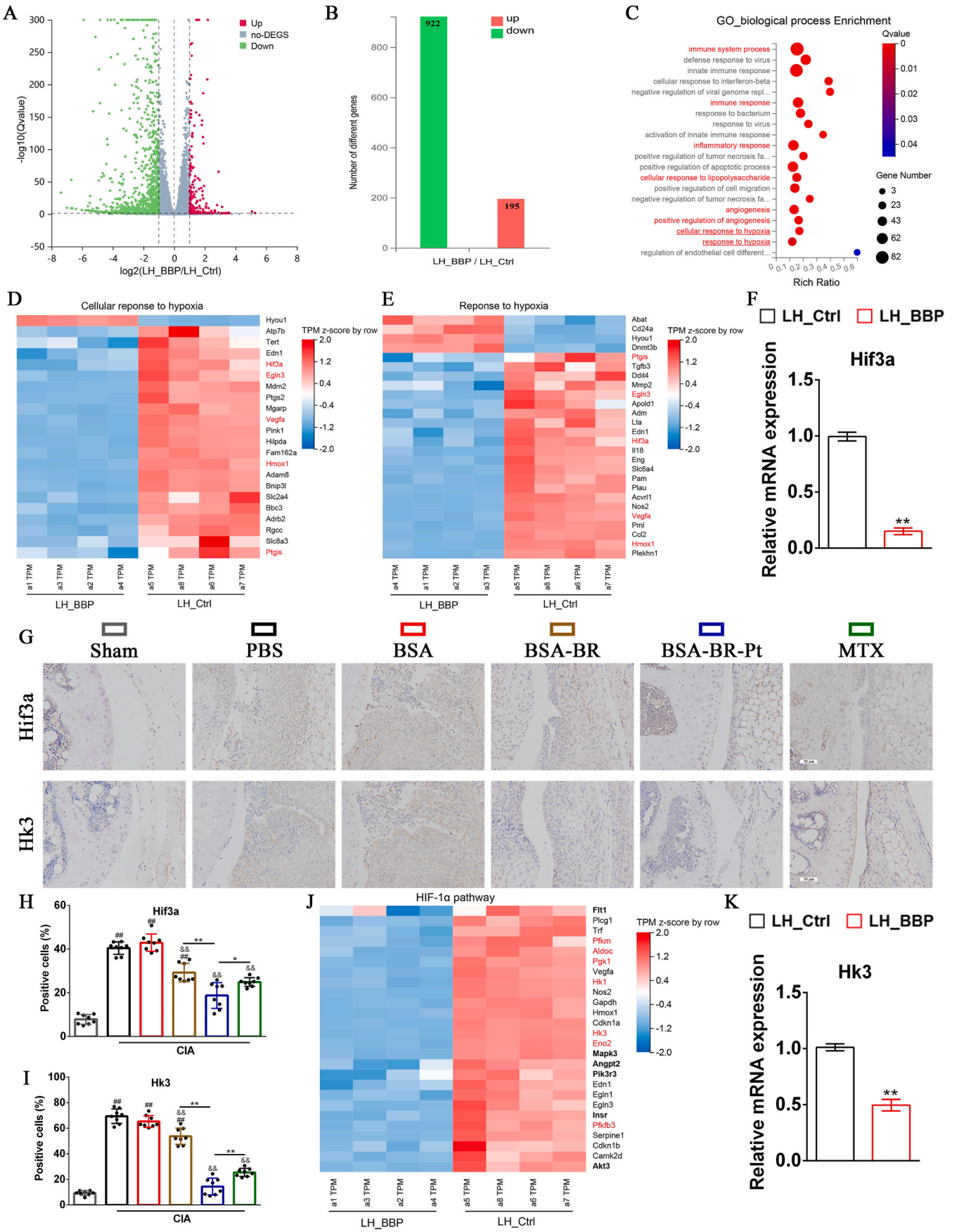

(caption on next page)

Fig. 9. RNA-seq analysis of hypoxic M1 polarized macrophages treated with BSA-BR-Pt NPs. **(A, B)** Volcano plot and number of DEGs of all genes identified in this study. Red and blue dots indicate up- or down-regulated genes significantly, respectively (|log2FC| ≥ 1 and Q-value of <0.05). **(C)** Representative GO analysis (biological process) of DEGs from LH_BBP vs. LH_Ctrl (|log2FC| ≥ 1 and Q-value of <0.05). **(D, E)** Heat map of DEGs from LH_BBP vs. LH_Ctrl in cellular response to hypoxia (D) and response to hypoxia (E) in the biological process. **(F)** qRT-PCR analysis of Hif3a mRNA expression in BMDMs from LH_BBP vs. LH_Ctrl. **(G–I)** Representative images and quantified analysis of Hif3a and Hk3 IHC staining in the synoivum of CIA mice with different treatment. Scale bar: 50 μm. **(J)** Heat map of DEGs from LH_BBP vs. LH_Ctrl in HIF-1α pathway. **(K)** qRT-PCR analysis of Hk3 mRNA expression in BMDMs from LH_BBP vs. LH_Ctrl. #, & and * indicate significant differences when compared with the sham, PBS, and BSA-BR-Pt NPs groups, respectively (*P < 0.05 and ##, &&, **P < 0.01).

expression of Vegfa in hypoxic M1 macrophages (Fig. S16B), indicating a potential role in mitigating these pathological changes to attenuate the development of RA. This result was also supported by a cluster analysis of DEGs in angiogenesis and positive regulation of angiogenesis, which demonstrated a significant inhibition of angiogenesis in the LH_BBP group when compared to the control, as shown in Figs. S18A and B. Subsequently, the findings from the human umbilical vein endothelial cells (HUVECs) tube formation assay showed that the cell supernantant derived from the LH_BPP group exhibited a obvious inhibitory effect on angiogenesis in comparison to the control group (Fig. S19). These findings suggested that hypoxic M1 macrophages reprogrammed with BSA-BR-Pt NPs effectively suppressed angiogenesis. Konisti et al. reported that the induction of angiogenesis in RA is probably a result of synovial hypoxia [32]. In the context of inflammation and hypoxia within the RA synovium, activated endothelial vessels facilitated the infiltration of inflammatory cells, resulting in the proliferation of synovial tissue. This process further strained oxygen supply, perpetuating a detrimental cycle that contributed to the progression of RA [37,38]. These evidences illustrated BSA-BR-Pt NPs effectively mitigated the development of RA by inhibiting the pro-angiogenic capacity of hypoxic M1 macrophages.

The analysis of KEGG enrichment showed that the DEGs in the LH_BBP vs. LH_Ctrl comparison were enriched in multiple pathways, such as cytokine-cytokine receptor interaction, rheumatoid arthritis, TNF signaling pathway, osteoclast differentiation, energy metabolism, p53signaling pathway, NOD-like receptor signaling pathway, JAK-STAT signaling pathway, and HIF-1 signaling pathway (Figs. S15B and S15C). Cluster analysis of DEGs involved in cytokine-cytokine receptor interaction, rheumatoid arthritis, TNF signaling pathway and osteoclast differentiation revealed a downregulation of pro-inflammatory cytokines (IL-1β, IL-18, Ccr9, Ccl2, Mmp9 and Tgfb3) [39,40] and bone resorption markers (Acp5 and Ctsk) [41] were observed in the LH_BBP group compared to the LH_Ctrl group (Figs. S20A–D). This indicated that BSA-BR-Pt NPs not only reduced the expression of inflammatory cytokines to alleviate synovitis but also inhibited osteoclast activity. The therapeutic effects of BSA-BR-Pt NPs in alleviating paw thickness, inhibiting synovial inflammation, reducing the number of osteoclasts and attenuating bone erosion in mice with CIA were similarly demonstrated (Figs. 6–8). Following this, the results from osteoclast TRAP staining assay and qRT-PCR analysis showed that the cell supernantant obtained from the LH_BPP group exhibited an obvious inhibitory impact on osteoclast activity *in vitro* when compared to the control group (Figs. S21A–D). Interestingly, the reduced osteoclast activity was also observed in osteoclasts treated with BSA-BR-Pt NPs in comparison to the control group (Figs. S21E–H).

Gene-set enrichment analysis (GSEA) revealed the LH_BBP group exhibited a significant downregulation of p53 signaling pathway, NOD-like receptor signaling pathway, JAK-STAT signaling pathway and HIF-1α pathway in comparison to the LH_Ctrl group (Figs. S22A–D). Prior research had reported that these signaling pathways were involved in the progression of RA [42–44]. In our investigation of the mechanisms by which BSA-BR-Pt NPs ameliorate hypoxia, we conducted cluster analysis to focus on DEGs in the HIF-1α pathway (Fig. 9J). The heatmaps of DEGs showed a significantly reduced expression of genes activating HIF-1α pathway (such as Flt1, Mapk3, Angpt2, Pik3r3, Insr and Akt3) [45–47] and genes associated with glycolysis (such as Pfkm, Aldoc, Pgk1, Hk1, Hk3, Eno2 and Pfkfb3) [48,49] in the LH_BBP group. The results from qRT-PCR analysis demonstrated that BSA-BR-Pt NPs treatment could reduced the mRNA expression levels of Mapk3, Angpt2, Pik3r3, Insr, Pfkm, Aldoc, Pgk1, Hk3, Eno2 and Pfkfb3, while no significant difference were observed in the mRNA expression levles of Flt1, Akt3 and Hk1 (Fig. 9K and Fig. S23A and B). Bustamante et al.It was previously stated that Hk2 is uniquely present in RA synovial lining and could be a promising metabolic target for the treatment of RA [50], however, the expression and role of Hk3 in RA were still unclear. We therefore performed IHC staining of Hk3 in synovial tissues of CIA mice treated with different NPs. The results revealed that markedly increased Hk3 positive cells were observed in synovium of CIA mice compared to the Sham group. BSA-BR NPs and MTX could effectively reduced the expression of Hk3 in hypoxia synovium, however they were no more effective effect than BSA-BR-Pt NPs (Fig. 9G and I). The extracellular acidification rate (ECAR) is a measure of glycolysis activity [51]. Compared to the control, obviously decreased ECAR were observed in hypoxia M1 macrophages with BSA-BR-Pt NPs treatment (Fig. S24A), suggesting BSA-BR-Pt NPs effectively inhibit glycolysis in hypoxia M1 macrophages. It was well-established that the downregulation of glycolysis-related genes and the suppression of glycolysis activity was beneficent for enhancing macrophage M2 polarization [13,52]. These findings offer evidence supporting the role and mechanism of BSA-BR-Pt NPs in hypoxic M1 macrophage reprogramming by inhibiting Hk3-mediated glycolysis activity. Furthermore, the classical M1 macrophage subtype is distinguished by elevated aerobic glycolysis and reduced oxidative phosphorylation (OXPHOS), whereas the M2 macrophage subtype is characterized by heightened OXPHOS [53–55]. The DEGs in OXPHOS were compared between LH_Ctrl and LH_BBP group by cluster analysis (Fig. S20E). The results from heatmap analysis indicatied that a total of 62 DEGs were identified, with 40 (64.52 %) showing identical downregulation and 22 (35.48 %) showing identical upregulation. These findings were further confirmed by qRT-PCR and measurement of oxygen consumption rate (OCR), a metric of OXPHOS activity [56]. The qRT-PCR results demonstrated an obvious increase in mRNA expression levels of key genes associated with OXPHOS (such as Ndufb8, Uqcrc1, Uqcrc2, Atp5a1 Sdha and Cox10) in hypoxic M1 macrophages treated with BSA-BR-Pt NPs compared to the control group (Fig. S23C). Additionally, OCR analysis revealed that BSA-BR-Pt NPs effectively enhanced the OXPHOS levels of hypoxic M1 macrophages (Fig. S24B). Collectively, these evidences suggested that BSA-BR-Pt NPs could switch cellular metabolism from glycolysis to OXPHOS through HIF-1α/HIF-3α/Hk3 pathway, ultimately reprogramming hypoxic M1 macrophages to M2 macrophages.

Nanomedicine is emerging as a promising approach in the realm of RA therapy, aiming to mitigate the pronounced side effects associated with conventional anti-RA drugs and enhance the therapeutic effects [57–59]. Although our work and other studies have demonstrated that the synergistic improvement of hypoxia and elimination of ROS is an effective strategy for RA therapy [14,27,28,60], our findings further identified that M1-to-M2 re-polarized macrophages treated with BSA-BR-Pt NPs might impede the continuous bone resorption and aberrant angiogenesis during the progression of RA. Our study contributes to the broader application of this therapeutic strategy and offers a potential treatment for secondary complications in RA. Notably, we are the first to elucidate the intricate mechanisms of this therapeutic strategy in combating RA. This not only enhances the translational relevance of our findings but also paves the way for a broader spectrum of therapeutic interventions targeting RA and potentially other inflammatory disorders. However, the complex mechanisms of various

nanomedicine-based strategies necessitate further investigation. A deeper understanding of the mechanisms by which nanomedicine effectively mitigates the progression of RA may lead to the discovery of additional therapeutic targets and facilitate the clinical application of nanomedicine.

4. Conclusion

The detrimental feedback loop between hypoxia and oxidative stress is a key factor in reshaping macrophage polarization, thus aggravating the progression of RA. In this study, we engineered BSA-BR-Pt NPs with synergistic hypoxia-alleviating and ROS-scavenging properties to mitigate the progression of RA through microenvironmental modulation and macrophage reprogramming strategies. Our results demonstrate that BSA-BR-Pt NPs effectively generate O_2 and synergistically scavenge ROS *in vitro*. Importantly, the therapeutic effects are notably observed in the knee and ankle joints of CIA mice treated with BSA-BR-Pt NPs compared to MTX, as evidenced by significant reductions in paw thickness, joint diameter, synovitis score, Mankin score, and bone erosion area. Mechanistically, BSA-BR-Pt NPs reprogram hypoxic M1 macrophages to M2 macrophages by switching glycolysis to OXPHOS via HIF-1a pathway. In summary, we fabricated an effective anti-RA enzyme-catalyzed nanoplatform with a combination of gas treatment and antioxidant therapy, illuminated its underlying mechanism, and proposed a promising therapeutic strategy for RA by interrupting the detrimental feedback loop between hypoxia and oxidative stress to reprogram macrophage polarization. Furthermore, this work provides guidance for the development of enzyme-catalyzed nanoplatform with synergistic hypoxia-relieving and ROS-scavenging properties for treating RA and other inflammatory disorders.

Funding statement

Funding for this project was provided by the National Natural Science Foundation of China (No. 81974328, 82372358, 82072443 and 82372425), the Natural Science Foundation for Distinguished Young Scholars of Guangdong Province (2022B1515020044) and Guangdong Students' Platform for Innovation and Entrepreneurship Training Program (S202312121083). The authors would also like to acknowledge the ICP-OES analysis provided by zkec (www.zkec.cc).

Data availability statement

The data underpinning the conclusions of this study can be found in the main text and supplementary materials of the publication. All data produced during the course of this research are encompassed within this article and its supplementary information appendices. Access to the data from this study can be obtained by contacting the corresponding author with a reasonable inquiry.

Ethics approval and consent to participate

The animal experiments were approved by the Animal Experimental Committee of the Daoke Pharmaceutical Technology (Guangdong) Co., Ltd (Approval IACUC-DK-2024-04-22-01) and were conducted in compliance with the guidelines stipulated in the National Act on the Use of Experimental Animals (People's Republic of China).

CRediT authorship contribution statement

Dong Guo: Writing – original draft, Visualization, Investigation, Formal analysis, Data curation, Conceptualization. **Hui Liu:** Writing – original draft, Visualization, Software, Data curation, Conceptualization. **Sheng Zhao:** Software, Formal analysis, Data curation. **Xinya Lu:** Validation, Resources, Methodology. **Haoyu Wan:** Software, Investigation. **Yitao Zhao:** Visualization, Investigation. **Xinzhi Liang:** Methodology, Investigation. **Anbiao Zhang:** Validation, Resources. **Mengyuan Wu:** Software, Data curation. **Zhisheng Xiao:** Methodology. **Ning Hu:** Funding acquisition. **Zhong Li:** Investigation. **Denghui Xie:** Writing – review & editing, Supervision, Project administration, Funding acquisition, Conceptualization.

Declaration of competing interest

The authors assert that the research was carried out without any commercial or financial affiliations that could be perceived as a possible conflict of interest. Fig. 6A is created using Figdraw (www.figdraw.com).

Appendix A. Supplementary data

Supplementary data to this article can be found online at https://doi.org/10.1016/j.bioactmat.2024.07.026.

References

[1] W. Geng, J. Zhao, B. Tao, Y. Yang, Q. Duan, P. Gao, T. He, S. Liu, Q. Feng, P. Zhao, K. Cai, Regulation of rheumatoid arthritis microenvironment via a self-healing injectable hydrogel for improved inflammation elimination and bone repair, Bioact. Mater. 36 (2024) 287–300, https://doi.org/10.1016/j.bioactmat.2024.03.002.

[2] W. Geng, X. Liu, B. Tao, Y. He, K. Li, P. Gao, Q. Feng, P. Zhao, Z. Luo, K. Cai, Nitric Oxide scavenging and hydrogen Sulfide production synergistically Treat rheumatoid arthritis, Adv. Healthcare Mater. 12 (4) (2023) e2202380, https://doi.org/10.1002/adhm.202202380.

[3] Y. Xu, Y. Li, A. Gao, P.K. Chu, H. Wang, Gasotransmitter delivery for bone diseases and regeneration, The Innovation Life 1 (1) (2023) 100015, https://doi.org/10.59717/j.xinn-life.2023.100015.

[4] R. Huang, C. Zhang, Y. Bu, Z. Li, X. Zheng, S. Qiu, J.O. Machuki, L. Zhang, Y. Yang, K. Guo, F. Gao, A multifunctional nano-therapeutic platform based on octahedral yolk-shell Au NR@CuS: Photothermal/photodynamic and targeted drug delivery tri-combined therapy for rheumatoid arthritis, Biomaterials 277 (2021) 121088, https://doi.org/10.1016/j.biomaterials.2021.121088.

[5] S. Alivernini, G.S. Firestein, I.B. McInnes, The pathogenesis of rheumatoid arthritis, Immunity 55 (12) (2022) 2255–2270, https://doi.org/10.1016/j.immuni.2022.11.009.

[6] N. Jia, Y. Gao, M. Li, Y. Liang, Y. Li, Y. Lin, S. Huang, Q. Lin, X. Sun, Q. He, Y. Yao, B. Zhang, Z. Zhang, L. Zhang, Metabolic reprogramming of proinflammatory macrophages by target delivered roburic acid effectively ameliorates rheumatoid arthritis symptoms, Signal Transduct. Targeted Ther. 8 (1) (2023) 280, https://doi.org/10.1038/s41392-023-01499-0.

[7] C. Li, C. Deng, S. Wang, X. Dong, B. Dai, W. Guo, Q. Guo, Y. Feng, H. Xu, X. Song, L. Cao, A novel role for the ROS-ATM-Chk2 axis mediated metabolic and cell cycle reprogramming in the M1 macrophage polarization, Redox Biol. 70 (2024) 103059, https://doi.org/10.1016/j.redox.2024.103059.

[8] U. Fearon, M. Canavan, M. Biniecka, D.J. Veale, Hypoxia, mitochondrial dysfunction and synovial invasiveness in rheumatoid arthritis, Nat. Rev. Rheumatol. 12 (7) (2016) 385–397, https://doi.org/10.1038/nrrheum.2016.69.

[9] C.T. Ng, M. Biniecka, A. Kennedy, J. McCormick, O. Fitzgerald, B. Bresnihan, D. Buggy, C.T. Taylor, J. O'Sullivan, U. Fearon, D.J. Veale, Synovial tissue hypoxia and inflammation in vivo, Ann. Rheum. Dis. 69 (7) (2010) 1389–1395, https://doi.org/10.1136/ard.2009.119776.

[10] T. Cramer, Y. Yamanishi, B.E. Clausen, I. Förster, R. Pawlinski, N. Mackman, V. H. Haase, R. Jaenisch, M. Corr, V. Nizet, G.S. Firestein, H.P. Gerber, N. Ferrara, R. S. Johnson, HIF-1alpha is essential for myeloid cell-mediated inflammation, Cell 112 (5) (2003) 645–657, https://doi.org/10.1016/s0092-8674(03)00154-5.

[11] T. McGarry, M. Biniecka, D.J. Veale, U. Fearon Hypoxia, Oxidative stress and inflammation, Free Radic. Biol. Med. 125 (2018) 15–24, https://doi.org/10.1016/j.freeradbiomed.2018.03.042.

[12] E. Brouwer, A.S. Gouw, M.D. Posthumus, M.A. van Leeuwen, A.L. Boerboom, J. Bijzet, R. Bos, P.C. Limburg, C.G. Kallenberg, J. Westra, Hypoxia inducible factor-1-alpha (HIF-1alpha) is related to both angiogenesis and inflammation in rheumatoid arthritis, Clin. Exp. Rheumatol. 27 (6) (2009) 945–951.

[13] J. Blagih, R.G. Jones, Polarizing macrophages through reprogramming of glucose metabolism, Cell Metabol. 15 (6) (2012) 793–795, https://doi.org/10.1016/j.cmet.2012.05.008.

[14] Y. Yang, L. Guo, Z. Wang, P. Liu, X. Liu, J. Ding, W. Zhou, Targeted silver nanoparticles for rheumatoid arthritis therapy via macrophage apoptosis and Re-polarization, Biomaterials 264 (2021) 120390, https://doi.org/10.1016/j.biomaterials.2020.120390.

[15] R.B. Vega, J.L. Horton, D.P. Kelly, Maintaining ancient organelles: mitochondrial biogenesis and maturation, Circ. Res. 116 (11) (2015) 1820–1834, https://doi.org/10.1161/CIRCRESAHA.116.305420.

[16] T.W. Kim, Y. Kim, W. Jung, D.E. Kim, H. Keum, Y. Son, S. Jon, Bilirubin nanomedicine ameliorates the progression of experimental autoimmune

encephalomyelitis by modulating dendritic cells, J. Contr. Release 331 (2021) 74–84, https://doi.org/10.1016/j.jconrel.2021.01.019.
[17] Y. Lee, H. Kim, S. Kang, J. Lee, J. Park, S. Jon, Bilirubin nanoparticles as a nanomedicine for anti-inflammation therapy, Angew Chem. Int. Ed. Engl. 55 (26) (2016) 7460–7463, https://doi.org/10.1002/anie.201602525.
[18] Z. Chen, C.T. Vong, C. Gao, S. Chen, X. Wu, S. Wang, Y. Wang, Bilirubin nanomedicines for the treatment of reactive oxygen species (ROS)-Mediated diseases, Mol. Pharm. 17 (7) (2020) 2260–2274, https://doi.org/10.1021/acs.molpharmaceut.0c00337.
[19] Y. Zhang, F. Wang, C. Liu, Z. Wang, L. Kang, Y. Huang, K. Dong, J. Ren, X. Qu, Nanozyme decorated Metal-Organic Frameworks for enhanced photodynamic therapy, ACS Nano 12 (1) (2018) 651–661, https://doi.org/10.1021/acsnano.7b07746.
[20] X.L. Liu, X. Dong, S.C. Yang, X. Lai, H.J. Liu, Y. Gao, H.Y. Feng, M.H. Zhu, Y. Yuan, Q. Lu, J.F. Lovell, H.Z. Chen, C. Fang, Biomimetic Liposomal Nanoplatinum for targeted cancer Chemophototherapy, Adv. Sci. 8 (8) (2021) 2003679, https://doi.org/10.1002/advs.202003679.
[21] D. Guo, C. Lin, Y. Lu, H. Guan, W. Qi, H. Zhang, Y. Shao, C. Zeng, R. Zhang, H. Zhang, X. Bai, D. Cai, FABP4 secreted by M1-polarized macrophages promotes synovitis and angiogenesis to exacerbate rheumatoid arthritis, Bone Res 10 (1) (2022) 45, https://doi.org/10.1038/s41413-022-00211-2.
[22] H. Shen, L. Jin, Q. Zheng, Z. Ye, L. Cheng, Y. Wu, H. Wu, T.G. Jon, W. Liu, Z. Pan, Z. Mao, Y. Wang, Synergistically targeting synovium STING pathway for rheumatoid arthritis treatment, Bioact. Mater. 24 (2023) 37–53, https://doi.org/10.1016/j.bioactmat.2022.12.001.
[23] D. Guo, H. Pan, X. Lu, Z. Chen, L. Zhou, S. Chen, J. Huang, X. Liang, Z. Xiao, H. Zeng, Y. Shao, W. Qi, D. Xie, C. Lin, Rspo2 exacerbates rheumatoid arthritis by targeting aggressive phenotype of fibroblast-like synoviocytes and disrupting chondrocyte homeostasis via Wnt/β-catenin pathway, Arthritis Res. Ther. 25 (1) (2023) 217, https://doi.org/10.1186/s13075-023-03198-1.
[24] J.Y. Kim, D.Y. Lee, S. Kang, W. Miao, H. Kim, Y. Lee, S. Jon, Bilirubin nanoparticle preconditioning protects against hepatic ischemia-reperfusion injury, Biomaterials 133 (2017) 1–10, https://doi.org/10.1016/j.biomaterials.2017.04.011.
[25] C.M. Quiñonez-Flores, S.A. González-Chávez, C. Pacheco-Tena, Hypoxia and its implications in rheumatoid arthritis, J. Biomed. Sci. 23 (1) (2016) 62, https://doi.org/10.1186/s12929-016-0281-0.
[26] I.A. Udalova, A. Mantovani, M. Feldmann, Macrophage heterogeneity in the context of rheumatoid arthritis, Nat. Rev. Rheumatol. 12 (8) (2016) 472–485, https://doi.org/10.1038/nrrheum.2016.91.
[27] C. Xu, Y. Jiang, H. Wang, Y. Zhang, Y. Ye, H. Qin, J. Gao, Q. Dan, L. Du, L. Liu, F. Peng, Y. Li, Y. Tu, Arthritic microenvironment Actuated Nanomotors for active rheumatoid arthritis therapy, Adv. Sci. 10 (4) (2023) e2204881, https://doi.org/10.1002/advs.202204881.
[28] J. Kim, H.Y. Kim, S.Y. Song, S.H. Go, H.S. Sohn, S. Baik, M. Soh, K. Kim, D. Kim, H. C. Kim, N. Lee, B.S. Kim, T. Hyeon, Synergistic oxygen generation and reactive oxygen species scavenging by Manganese Ferrite/Ceria Co-decorated nanoparticles for rheumatoid arthritis treatment, ACS Nano 13 (3) (2019) 3206–3217, https://doi.org/10.1021/acsnano.8b08785.
[29] A. Di Matteo, J.M. Bathon, P. Emery, Rheumatoid arthritis, Lancet 402 (10416) (2023) 2019–2033, https://doi.org/10.1016/S0140-6736(23)01525-8.
[30] R.E. Toes, K. Raza, The autoimmune response as a potential target for tolerance induction before the development of rheumatoid arthritis, Lancet Rheumatol 3 (3) (2021) e214–e223, https://doi.org/10.1016/S2665-9913(20)30445-8.
[31] W. Gao, J. McCormick, M. Connolly, E. Balogh, D.J. Veale, U. Fearon, Hypoxia and STAT3 signalling interactions regulate pro-inflammatory pathways in rheumatoid arthritis, Ann. Rheum. Dis. 74 (6) (2015) 1275–1283, https://doi.org/10.1136/annrheumdis-2013-204105.
[32] S. Konisti, S. Kiriakidis, E.M. Paleolog, Hypoxia–a key regulator of angiogenesis and inflammation in rheumatoid arthritis, Nat. Rev. Rheumatol. 8 (3) (2012) 153–162, https://doi.org/10.1038/nrrheum.2011.205.
[33] E.L. Kerber, C. Padberg, N. Koll, V. Schuetzhold, J. Fandrey, S. Winning, The Importance of hypoxia-inducible factors (HIF-1 and HIF-2) for the Pathophysiology of inflammatory Bowel disease, Int. J. Mol. Sci. 21 (22) (2020), https://doi.org/10.3390/ijms21228551.
[34] Y. He, X. Liu, J. De, S. Kang, J.S. Munday, Altered hypoxia-induced and Heat Shock protein immunostaining in secondary Hair Follicles associated with changes in Altitude and temperature in Tibetan Cashmere Goats, Animals 11 (10) (2021), https://doi.org/10.3390/ani11102798.
[35] K.J. Cheng, Y.Y. Bao, S.H. Zhou, The role of hypoxia inducible factor in nasal inflammations, Eur. Rev. Med. Pharmacol. Sci. 20 (24) (2016) 5067–5076.
[36] J. Avouac, S. Pezet, E. Vandebeuque, C. Orvain, V. Gonzalez, G. Marin, G. Mouterde, C. Daïen, Y. Allanore Semaphorins, From angiogenesis to inflammation in rheumatoid arthritis, Arthritis Rheumatol. 73 (9) (2021) 1579–1588, https://doi.org/10.1002/art.41701.
[37] H.A. Elshabrawy, Z. Chen, M.V. Volin, S. Ravella, S. Virupannavar, S. Shahrara, The pathogenic role of angiogenesis in rheumatoid arthritis, Angiogenesis 18 (4) (2015) 433–448, https://doi.org/10.1007/s10456-015-9477-2.
[38] A. Meyer, S.R. Zack, W. Nijim, A. Burgos, V. Patel, B. Zanotti, M.V. Volin, M. A. Amin, M.J. Lewis, C. Pitzalis, S. Arami, J.A. Karam, N.J. Sweiss, S. Shahrara, Metabolic reprogramming by Syntenin-1 directs RA FLS and endothelial cell-mediated inflammation and angiogenesis, Cell. Mol. Immunol. 21 (1) (2024) 33–46, https://doi.org/10.1038/s41423-023-01108-8.
[39] M. Noack, P. Miossec, Selected cytokine pathways in rheumatoid arthritis, Semin. Immunopathol. 39 (4) (2017) 365–383, https://doi.org/10.1007/s00281-017-0619-z.
[40] G. Hernandez, T.S. Mills, J.L. Rabe, J.S. Chavez, S. Kuldanek, G. Kirkpatrick, L. Noetzli, W.K. Jubair, M. Zanche, J.R. Myers, B.M. Stevens, C.J. Fleenor, B. Adane, C.A. Dinarello, J. Ashton, C.T. Jordan, J. Di Paola, J.R. Hagman, V. M. Holers, K.A. Kuhn, E.M. Pietras, Pro-inflammatory cytokine blockade attenuates myeloid expansion in a murine model of rheumatoid arthritis, Haematologica 105 (3) (2020) 585–597, https://doi.org/10.3324/haematol.2018.197210.
[41] K. Murata, C. Fang, C. Terao, E.G. Giannopoulou, Y.J. Lee, M.J. Lee, S.H. Mun, S. Bae, Y. Qiao, R. Yuan, M. Furu, H. Ito, K. Ohmura, S. Matsuda, T. Mimori, F. Matsuda, K.H. Park-Min, L.B. Ivashkiv, Hypoxia-sensitive COMMD1 Integrates signaling and cellular metabolism in human macrophages and Suppresses Osteoclastogenesis, Immunity 47 (1) (2017) 66–79.e5, https://doi.org/10.1016/j.immuni.2017.06.018.
[42] Q. Ding, W. Hu, R. Wang, Q. Yang, M. Zhu, M. Li, J. Cai, P. Rose, J. Mao, Y.Z. Zhu, Signaling pathways in rheumatoid arthritis: implications for targeted therapy, Signal Transduct. Targeted Ther. 8 (1) (2023) 68, https://doi.org/10.1038/s41392-023-01331-9.
[43] G. Salvador, R. Sanmarti, A. Garcia-Peiró, J.R. Rodríguez-Cros, J. Muñoz-Gómez, J. D. Cañete, p53 expression in rheumatoid and psoriatic arthritis synovial tissue and association with joint damage, Ann. Rheum. Dis. 64 (2) (2005) 183–187, https://doi.org/10.1136/ard.2004.024430.
[44] X. Liu, R. Guo, S. Huo, H. Chen, Q. Song, G. Jiang, Y. Yu, J. Huang, S. Xie, X. Gao, L. Lu, CaP-based anti-inflammatory HIF-1α siRNA-encapsulating nanoparticle for rheumatoid arthritis therapy, J. Contr. Release 343 (2022) 314–325, https://doi.org/10.1016/j.jconrel.2022.01.029.
[45] G.N. Masoud, W. Li, HIF-1α pathway: role, regulation and intervention for cancer therapy, Acta Pharm. Sin. B 5 (5) (2015) 378–389, https://doi.org/10.1016/j.apsb.2015.05.007.
[46] T. Sasagawa, T. Nagamatsu, K. Morita, N. Mimura, T. Iriyama, T. Fujii, M. Shibuya, HIF-2α, but not HIF-1α, mediates hypoxia-induced up-regulation of Flt-1 gene expression in placental trophoblasts, Sci. Rep. 8 (1) (2018) 17375, https://doi.org/10.1038/s41598-018-35745-1.
[47] J. Korbecki, D. Simińska, M. Gąssowska-Dobrowolska, J. Listos, I. Gutowska, D. Chlubek, I. Baranowska-Bosiacka, Chronic and cycling hypoxia: Drivers of cancer chronic inflammation through HIF-1 and NF-κB activation: a review of the molecular mechanisms, Int. J. Mol. Sci. 22 (19) (2021), https://doi.org/10.3390/ijms221910701.
[48] D. Du, C. Liu, M. Qin, X. Zhang, T. Xi, S. Yuan, H. Hao, J. Xiong, Metabolic dysregulation and emerging therapeutical targets for hepatocellular carcinoma, Acta Pharm. Sin. B 12 (2) (2022) 558–580, https://doi.org/10.1016/j.apsb.2021.09.019.
[49] T. Pan, S. Sun, Y. Chen, R. Tian, E. Chen, R. Tan, X. Wang, Z. Liu, J. Liu, H. Qu, Immune effects of PI3K/Akt/HIF-1α-regulated glycolysis in polymorphonuclear neutrophils during sepsis, Crit. Care 26 (1) (2022) 29, https://doi.org/10.1186/s13054-022-03893-6.
[50] M.F. Bustamante, P.G. Oliveira, R. Garcia-Carbonell, A.P. Croft, J.M. Smith, R. L. Serrano, E. Sanchez-Lopez, X. Liu, T. Kisseleva, N. Hay, C.D. Buckley, G. S. Firestein, A.N. Murphy, S. Miyamoto, M. Guma, Hexokinase 2 as a novel selective metabolic target for rheumatoid arthritis, Ann. Rheum. Dis. 77 (11) (2018) 1636–1643, https://doi.org/10.1136/annrheumdis-2018-213103.
[51] C.M. Klinge, Estrogenic control of mitochondrial function, Redox Biol. 31 (2020) 101435, https://doi.org/10.1016/j.redox.2020.101435.
[52] S.M. Morrissey, F. Zhang, C. Ding, D.E. Montoya-Durango, X. Hu, C. Yang, Z. Wang, F. Yuan, M. Fox, H.G. Zhang, H. Guo, D. Tieri, M. Kong, C.T. Watson, R.A. Mitchell, X. Zhang, K.M. McMasters, J. Huang, J. Yan, Tumor-derived exosomes drive immunosuppressive macrophages in a pre-metastatic niche through glycolytic dominant metabolic reprogramming, Cell Metabol. 33 (10) (2021) 2040–2058.e10, https://doi.org/10.1016/j.cmet.2021.09.002.
[53] G.M. Tannahill, A.M. Curtis, J. Adamik, E.M. Palsson-McDermott, A.F. McGettrick, G. Goel, C. Frezza, N.J. Bernard, B. Kelly, N.H. Foley, L. Zheng, A. Gardet, Z. Tong, S.S. Jany, S.C. Corr, M. Haneklaus, B.E. Caffrey, K. Pierce, S. Walmsley, F. C. Beasley, E. Cummins, V. Nizet, M. Whyte, C.T. Taylor, H. Lin, S.L. Masters, E. Gottlieb, V.P. Kelly, C. Clish, P.E. Auron, R.J. Xavier, L.A. O'Neill, Succinate is an inflammatory signal that induces IL-1β through HIF-1α, Nature 496 (7444) (2013) 238–242, https://doi.org/10.1038/nature11986.
[54] E.L. Mills, B. Kelly, A. Logan, A. Costa, M. Varma, C.E. Bryant, P. Tourlomousis, J. Däbritz, E. Gottlieb, I. Latorre, S.C. Corr, G. McManus, D. Ryan, H.T. Jacobs, M. Szibor, R.J. Xavier, T. Braun, C. Frezza, M.P. Murphy, L.A. O'Neill, Succinate Dehydrogenase supports metabolic Repurposing of Mitochondria to drive inflammatory macrophages, Cell 167 (2) (2016) 457–470.e13, https://doi.org/10.1016/j.cell.2016.08.064.
[55] S.C. Huang, B. Everts, Y. Ivanova, D. O'Sullivan, M. Nascimento, A.M. Smith, W. Beatty, L. Love-Gregory, W.Y. Lam, C.M. O'Neill, C. Yan, H. Du, N.A. Abumrad, J.J. Urban, M.N. Artyomov, E.L. Pearce, E.J. Pearce, Cell-intrinsic lysosomal lipolysis is essential for alternative activation of macrophages, Nat. Immunol. 15 (9) (2014) 846–855, https://doi.org/10.1038/ni.2956.
[56] S.K. Wculek, I. Heras-Murillo, A. Mastrangelo, D. Mañanes, M. Galán, V. Miguel, A. Curtabbi, C. Barbas, N.S. Chandel, J.A. Enríquez, S. Lamas, D. Sancho, Oxidative phosphorylation selectively orchestrates tissue macrophage homeostasis, Immunity 56 (3) (2023) 516–530.e9, https://doi.org/10.1016/j.immuni.2023.01.011.
[57] Y. Han, S. Huang, Nanomedicine is more than a supporting role in rheumatoid arthritis therapy, J. Contr. Release 356 (2023) 142–161, https://doi.org/10.1016/j.jconrel.2023.02.035.
[58] P. Hua, R. Liang, S. Yang, Y. Tu, M. Chen, Microneedle-assisted dual delivery of PUMA gene and celastrol for synergistic therapy of rheumatoid arthritis through

restoring synovial homeostasis, Bioact. Mater. 36 (2024) 83–95, https://doi.org/10.1016/j.bioactmat.2024.02.030.

[59] L. Zhang, Z. Qin, H. Sun, X. Chen, J. Dong, S. Shen, L. Zheng, N. Gu, Q. Jiang, Nanoenzyme engineered neutrophil-derived exosomes attenuate joint injury in advanced rheumatoid arthritis via regulating inflammatory environment, Bioact. Mater. 18 (2022) 1–14, https://doi.org/10.1016/j.bioactmat.2022.02.017.

[60] F. Zhou, M. Li, M. Chen, M. Chen, X. Chen, Z. Luo, K. Cai, Y. Hu, Redox homeostasis strategy for inflammatory macrophage reprogramming in rheumatoid arthritis based on Ceria Oxide nanozyme-Complexed Biopolymeric Micelles, ACS Nano 17 (5) (2023) 4358–4372, https://doi.org/10.1021/acsnano.2c09127.